RI 9027

Bureau of Mines Report of Investigations/1986

Shield Mechanics and Resultant Load Vector Studies

By Thomas M. Barczak and Robert C. Garson

UNITED STATES DEPARTMENT OF THE INTERIOR

Report of Investigations 9027

Shield Mechanics and Resultant Load Vector Studies

By Thomas M. Barczak and Robert C. Garson

UNITED STATES DEPARTMENT OF THE INTERIOR
Donald Paul Hodel, Secretary

BUREAU OF MINES
Robert C. Horton, Director

UNIT OF MEASURE ABBREVIATIONS USED IN THIS REPORT

deg	degree	min	minute
ft	foot	mm	millimeter
h	hour	pct	percent
in	inch	psi	pound per square inch
kV•A	kilovolt ampere	V	volt
lb	pound		

Library of Congress Cataloging in Publication Data:

Barczak, Thomas M

Shield mechanics and resultant load vector studies.

(Bureau of Mines report of investigations ; 9027)

Bibliography: p. 42.

Supt. of Docs. no.: I 28.23:9027.

1. Mine roof control. 2. Longwall mining. I. Garson, Robert C. II. Title. III. Series: Report of investigations (United States. Bureau of Mines) ; 9027.

TN23.U43 [TN288] 622s [622'.28] 85-600351

CONTENTS

ILLUSTRATIONS

ILLUSTRATIONS--Continued

TABLES

SHIELD MECHANICS AND RESULTANT LOAD VECTOR STUDIES

By Thomas M. Barczak[1] and Robert C. Garson[2]

ABSTRACT

The term "resultant load vector" is defined as the representation of the forces applied to a longwall roof support element by strata activity through a single, quantifiable measure of support resistance. The relatively complex kinematics of the shield structure prohibits determination of support resistance simply from the summation of leg forces. In the research reported in this Bureau of Mines study, the mechanics of the shield structure were evaluated, and a technique was developed whereby the resultant shield loading could be determined by instrumenting supports with pressure transducers and strain gauges to measure leg, canopy capsule, and lemniscate link forces. This technique has been laboratory tested in the Bureau's Mine Roof Simulator. Functional relationships among variables were assessed, and confidence intervals were established for prediction of the resultant load vector parameters. Resultant load measurements were taken on five instrumented shields on an active longwall face in Colorado. Results were analyzed and found to be consistent with shield mechanics and anticipated roof behavior. Benefits to be derived from this research, future efforts, and long-range goals are discussed.

[1]Physicist, Pittsburgh Research Center, Bureau of Mines, Pittsburgh, PA.
[2]Civil engineer, Boeing Services International, Pittsburgh, PA.

INTRODUCTION

Longwall mining is a capital-intensive system that requires increased dependence upon single production units. Current costs to equip a modern longwall system can easily exceed $10 million, with 40 to 60 pct of this cost attributable to the powered roof support system. Better design, selection, and utilization of the powered roof support system should reduce the capital required while improving the production, health, and safety performance for the longwall operator.

While the importance of proper ground control to successful longwall mining is recognized, the science of roof control and the interaction of the powered roof support system with the interburden strata remain largely unknown. Because of inadequate roof control and subsequent failures of several early longwall attempts in the United States, which utilized low-capacity European support equipment, there has been a tendency to increase support capacity with little regard to expected support loading. Since the cost of a support is related to its capacity, the use of excessively large supports represents an unnecessary capital investment and may cause unnecessary fracturing of the roof strata, thereby being detrimental to good roof control.

Several types of powered roof supports exist, although the shield design has gained prominence since its introduction into the United States around 1970. The shield design is characterized by the presence of a caving shield, which acts as a connecting structure from the canopy to the base, making the structure stable and able to resist horizontal loading. It is this feature, however, that makes the shield design more complex than the prior generations of frame-and-chock-type supports from a kinematic viewpoint, and prevents a determination of support resistance simply from the summation of leg forces alone.

Much can be learned about the science of roof behavior and strata mechanics from the behavior of the powered roof support system. The design of more effective roof support systems will only be realized once the interaction between the roof support system and the interburden is fully understood. In this sense, the roof support hardware can serve as the instrumentation (a giant load cell if you wish) by which roof behavior can be monitored and supoprt requirements established to effectively maintain the desired ground control. To effectively utilize the roof support hardware as a "load cell" to measure roof loading, the mechanics of the roof support structure must be understood in order to interpret the reaction of the support to applied roof loadings.

A fundamental measure of support resistance can be defined as the resultant load vector, which is the representation of all the forces applied to a longwall roof support element by strata activity into a single, quantifiable measure of support resistance (1).[3] Being a vector, this measure possesses not only a magnitude, but spatial parameters of location and direction as depicted in figure 1. Reference will be made to these three resultant load vector parameters:

1. Magnitude - magnitude of loading.
2. Location - position of resultant force acting on the canopy measured from the canopy hinge pin along the length of the canopy.

[3]Underlined numbers in parentheses refer to items in the list of references at the end of this report.

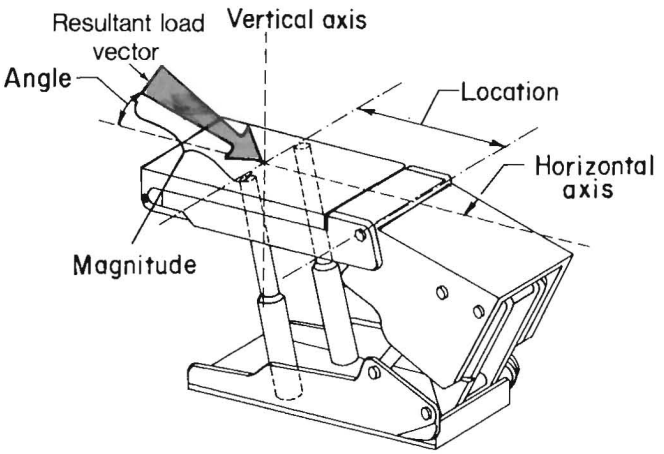

FIGURE 1. - Illustrations of resultant load vector concept.

3. Angle - inclination of the load vector normal to the plane of the canopy.

From these parameters, critical design information can be ascertained. For example, by knowing the magnitude and angle of the resultant vector, the magnitude of horizontal (face-to-waste) shield load can be assessed. Likewise, insight into the caving behavior of the strata can be gained by examination of the resultant location as it moves forward or rearward during the mining cycle. Coefficients of friction between the roof and canopy can be determined from the resultant angle and provide insight into the interaction of the support element with the immediate strata.

While it is recognized that resultant load vector information must be considered as baseline engineering data, the Bureau's Mine Roof Simulator (MRS) enables such information to be further analyzed under controlled laboratory conditions. The MRS (fig. 2) is a massive, bidirectional, hydraulic press capable of applying 1,500 tons of vertical force and 800 tons of horizontal force, either independently or simultaneously, to full-scale roof support elements (2). A load profile measured underground can be programmed into the MRS computer and simulated by the test rig. This enables comprehensive structural analysis of the support under controlled laboratory conditions and studies to evaluate such things as the effectiveness of the lemniscate design in resisting horizontal loading.

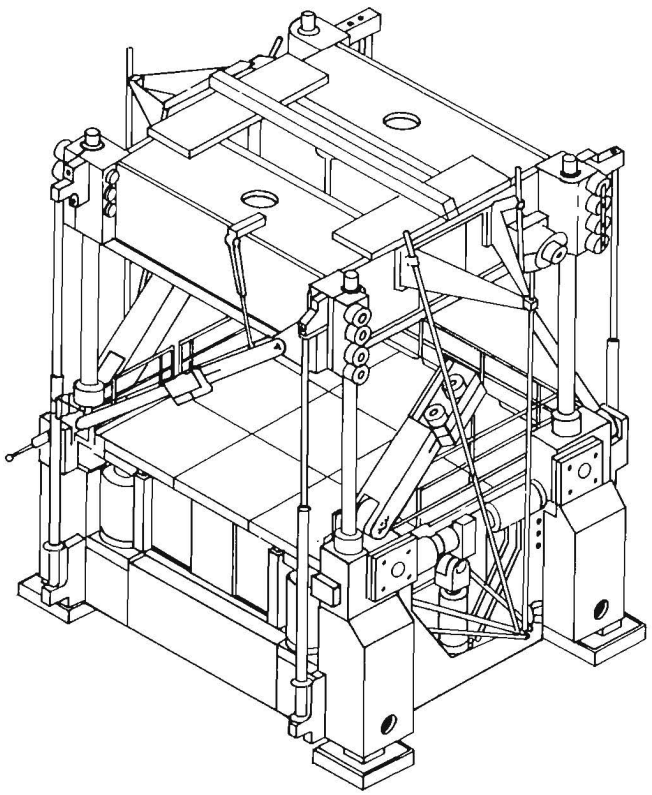

FIGURE 2. - Bureau's Mine Roof Simulator (MRS).

ACKNOWLEDGMENTS

The authors wish to acknowledge the services of Boeing Services International, Inc., Pittsburgh, PA, particularly the field crew consisting of Ed Hogue, Paul Kovscek, Karl Chulig, and others, who spent many long hours installing the instrumentation and collecting the data. Gratitude is also extended to Jay Reynolds and Snowmass Coal Co., and Carbondale Co. for their excellent cooperation and support of our research efforts at their mine site.

FUNCTIONAL BEHAVIOR OF SHIELD SUPPORTS

The shield design is characterized by four major components: (1) canopy, (2) caving shield, (3) hydraulic props, and (4) base. It is the caving shield, which in general is inclined and hinge-jointed to the canopy and base, that makes the shield a kinematically stable support to distinguish it from the chock and frame design. While there are many variations in the basic shield design (apart from the two-versus-four-leg considerations), the major differences are related to the orientation of the legs and the caving shield connection (3). The three primary leg orientations are shown in figure 3. The canopy connection, with the caving shield hinged at the rear of the canopy and the leg thrust applied directly to the canopy, is the most common type utilized today. In

terms of support efficiency, the hinge connection type is the most efficient. The three principal types of motional traces of the leading edge of the canopy are shown in figure 4. The lemniscate design has gained prominence in recent years because of the advantages offered by the vertical travel of the canopy during convergence, causing less disturbance to the roof strata during load application.

Although the variations in shield design are many, the two-leg, canopy-connected design with the lemniscate linkage system is probably the most common design currently utilized in longwall mining in the United States and will serve as the basis for this study. The major components of a basic two-leg shield (fig. 5) are identified and their functional reaction to applied loads is outlined in the following paragraphs:

1. Canopy - the roof beam that provides contact and support resistance to the roof strata.

2. Caving shield - connecting structure between the canopy and base that provides horizontal stability and protection from gob debris.

3. Compression lemniscate link - the forward link of the lemniscate linkage system.

4. Tension lemniscate link - the rear link of the lemniscate linkage system.

5. Base - the floor beam that provides contact and support resistance to the floor strata.

6. Leg cylinder - Single- or double-acting hydraulic prop that provides primary support thrust to the canopy.

7. Canopy capsule cylinder - double-acting hydraulic cylinder designed to provide control of the canopy attitude.

As indicated earlier, the primary basis for the design of the shield concept is its ability to resist horizontal (face-to-waste) roof loading. The reaction of the support under horizontal load is examined below. Figure 6 shows that the leg cylinder is inclined, providing a

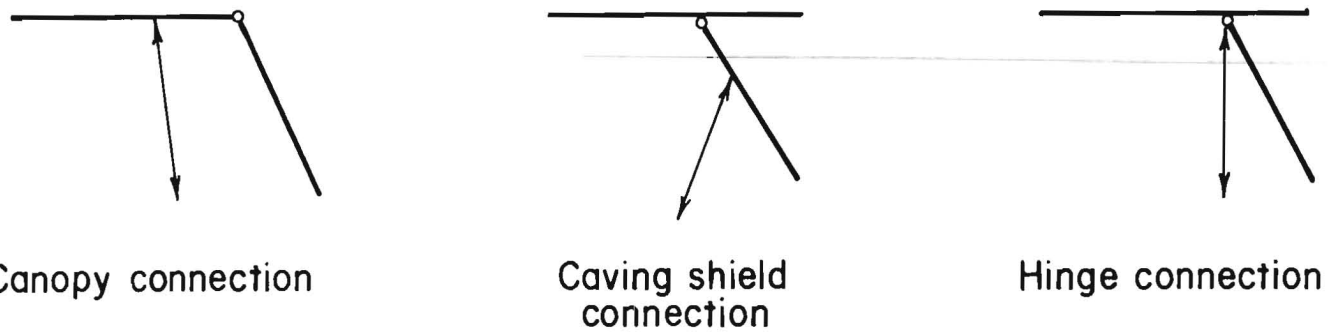

FIGURE 3. - Leg orientations for shield designs.

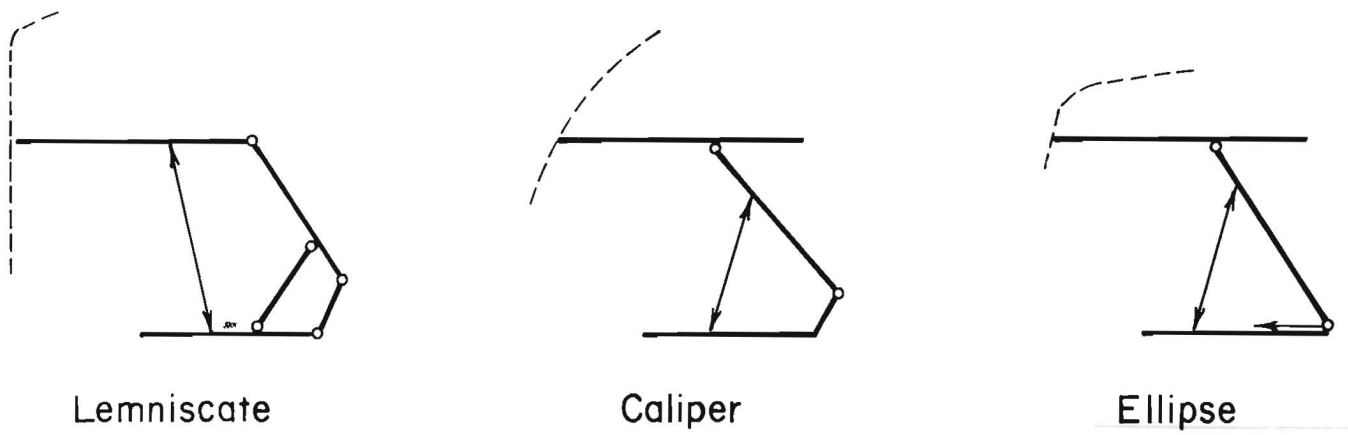

FIGURE 4. - Motional traces of canopy for shield designs.

horizontal component of support resistance (L*SIN α), which tries to push the canopy (point *A* in figure 6) toward the coal face. This motion of the canopy subsequently pulls on the caving shield and tries to push point *B* toward the face and point *C* toward the gob, putting the forward link in compression and the rear link in tension. As the leg force increases by reacting to an applied load, the degree of compression and tension in the appropriate lemniscate link increases proportionally.

If, however, there is an externally applied horizontal load by the strata (fig. 7), the opposite effect occurs, as the external force tries to cancel out the horizontal leg resistance and subsequently reduces link loading.

A more detailed analysis of the impact of horizontal loading can be ascertained from an examination of the forces acting on the canopy, as shown in figure 8. In terms of horizontal loading, the summation of the forces in horizontal (x) direction must equal zero to be consistent with the laws of physics.

$$\Sigma F(x) \rightarrow + = 0,$$

$$HORZ - L*SIN\ \alpha - N*SIN\ \theta + P_x = 0;$$

$$HORZ = L*SIN\ \alpha + N*SIN\ \theta - P_x, \qquad (1)$$

where HORZ = horizontal frictional force,

L*SIN α = horizontal component of leg force,

N*SIN θ = horizontal component of canopy capsule force,

and P_x = horizontal reaction at canopy hinge pin.

Depending upon the geometric configuration of the support, a static analysis

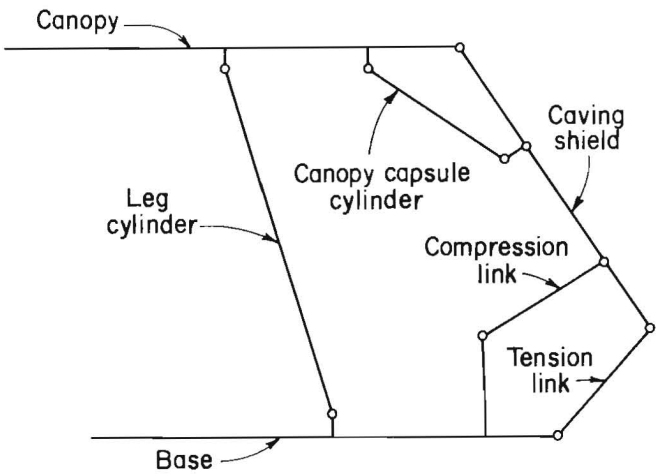

FIGURE 5. - Major components of two-leg shield.

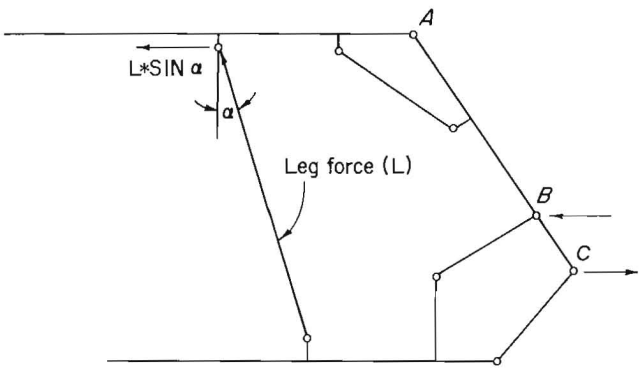

FIGURE 6. - Functional relationship of shield components and forces.

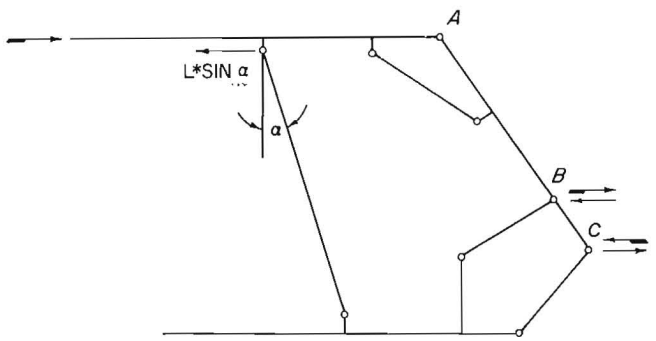

FIGURE 7. - Effect of externally applied horizontal load on shield behavior.

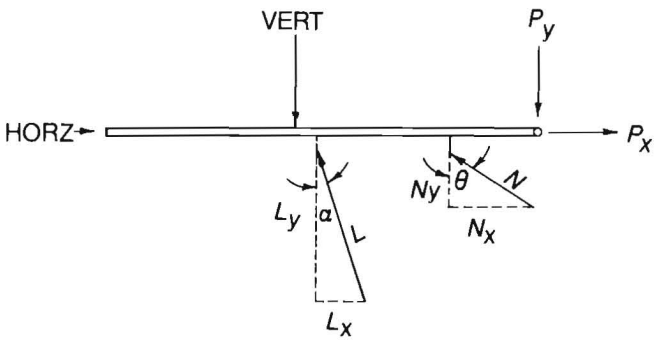

FIGURE 8. - Forces acting on shield canopy.

reveals that only a portion of the horizontal component of the leg resistance (L*SIN α) is converted into horizontal frictional force (HORZ) acting on the support. From equation 1 and examination of the forces acting on the canopy as shown in figure 8, it is seen that the reaction at the canopy hinge pin acts in the same direction as the frictional force (HORZ); hence part of the horizontal component of the leg and canopy capsule force is utilized to overcome the hinge pin force (P_x), and only a portion of these forces is converted into HORZ. For example, in a support with 342 tons of vertical force and 41 tons of horizontal frictional force (HORZ), 53 pct of the horizontal component of the leg force is utilized to negate the hinge pin force (P_x), if there is assumed to be no canopy capsule force. The addition of a canopy capsule force will cause the hinge pin force to increase, and since this increase is at a faster rate than that of the leg-capsule force combination, the addition of a capsule force causes a further reduction in the amount of leg force converted into frictional force (HORZ). For the previous example of 342 tons of vertical force and 41 tons of horizontal force, the addition of a capsule force of 27.73 tons will reduce the degree of leg force converted into horizontal frictional force from 47 pct to 37 pct. The case examined is considered to be representative of the mine loading observed on this support.

In terms of vertical support resistance, the presence of horizontal loading can increase or decrease support capacity, depending upon the geometry and operating height of the support (4). Mathematically, this can be seen from a static analysis of the forces employed on the support structure. As can be seen from figure 8, the forces in the vertical (y) direction acting on the canopy are summed to zero in accordance with the laws of static equilibrium.

$$\Sigma\ F(y)\ \uparrow\ +\ =\ 0,$$

$$-\text{VERT} + \text{L*COS}\ \alpha + \text{N*COS}\ \theta - P_y = 0. \qquad (2)$$

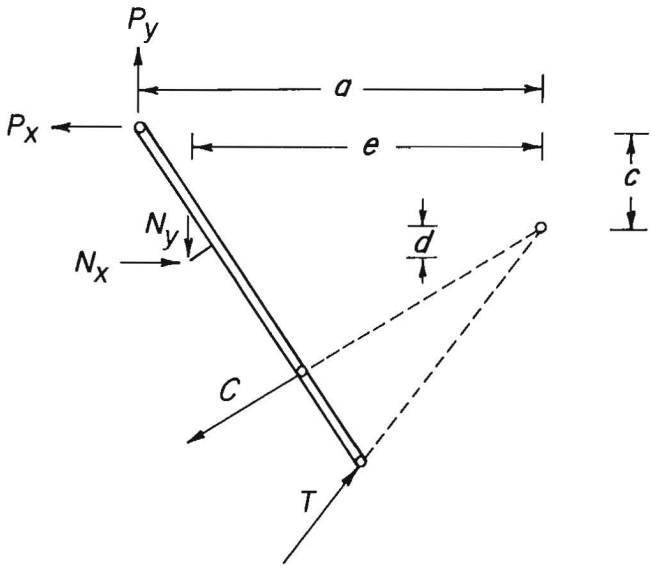

FIGURE 9. - Forces acting on caving shield.

From this, the support capacity (vertical support resistance) VERT is defined as follows:

$$\text{VERT} = \text{L*COS}\ \alpha + \text{N*COS}\ \theta - P_y. \qquad (3)$$

Examination of the forces acting on the caving shield reveals the following relationship by taking moments about the instantaneous center of the lemniscate links (fig. 9).

$$\Sigma\ M\ (I)\ \nearrow\ +\ =\ 0,$$

$$-P_x(c) + P_y(a) - N_x(d) - N_y(e) = 0, \qquad (4)$$

$$P_y = \frac{P_x(c) + N_x(d) + N_y(e)}{a}, \qquad (5)$$

where P_y = vertical reaction force at canopy hinge pin,

P_x = horizontal reaction force at canopy hinge pin,

N_x = horizontal component of canopy capsule force,

N_y = vertical component of canopy capsule force,

a = moment arm for P_y,

c = moment arm for P_x,

d = moment arm for N_x,

and e = moment arm for N_y.

Substituting P_y from equation 5 into equation 3, the vertical support resistance VERT is found as follows:

$$VERT = L*COS\ \alpha + N*COS\ \theta - \frac{P_x(c)}{a} - \frac{N_x(d) - N_y(e)}{a}. \quad (6)$$

The impact of horizontal loading is expressed by the term $P_x(c)/a$ since for pure vertical loading, this term becomes insignificant, approaching zero as the leg angle approaches 90°. Examination of this term reveals that the effect of horizontal load on support capacity is dependent upon the geometry of the support, in particular the location of the instantaneous center of the lemniscate links (point where the line of action of the axial lemniscate link forces meet) relative to the plane of the canopy. Further examination shows that for the horizontal force to have no effect on the load-carrying capacity of the support, c in equation 6 must be equal to zero (i.e., the canopy hinge must be level with the instantaneous center of the lemniscate links) to force the term $P_x(c)/a$ to zero. Since c is a moment arm in an equation of turning moments, the sense or sign of moment produced by c is important. In general, for a two-leg shield, if the instantaneous center of the lemniscate links falls below the level of the canopy, the effect of an external horizontal load will be to decrease the support load-carrying capacity since the term $P_x(c)/a$ is negative in equation 6. The magnitude of this reduction in capacity will be dependent upon the distance of the instantaneous link center from the plane of the canopy (c), which is determined by the shield height. Normally, the shield is designed to minimize this effect by keeping the instantaneous center as close to the canopy level as possible for the designated operating height of the support. On the other hand, if the instantaneous link center falls above the canopy level, the effect of horizontal load is to increase support capacity. As indicated, these statements are generalities and do not include all load cases that are possible. For example, if the resultant location is to the rear of the leg-canopy capsule resultant force, the direction of the vertical reaction at the canopy hinge is reversed and the opposite effect is observed from that previously discussed.

Horizontal loading is obviously an important consideration in the design of the shield support since it affects the overall load-carrying capability. However, the primary function of the support is to resist vertical (roof-to-floor) convergence. The primary means of support resistance is provided by the leg cylinders, but the canopy capsule plays an important role in controlling the attitude of the canopy and, subsequently, the location of the resultant load vector. Recalling the description of shield components presented earlier, the canopy capsule cylinder is a double-acting, hydraulic cyliner. Depending on the location of the resultant load vector, either the retract or the extend side will exert a controlling force to the canopy structure during load application. As can be seen from figure 10, a tip load or resultant force forward of the leg line will cause an increase in extend-side pressure as the canopy tries to rotate about the leg pivot and to reduce the included

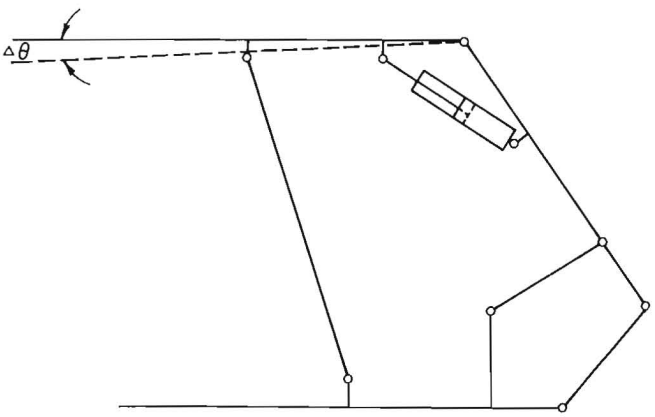

FIGURE 10. - Effect of tip load on canopy capsule behavior.

angle between the canopy and the caving shield. The opposite would occur with a resultant load rearward of the leg line, thus causing an increase in retract-side pressure. Likewise, vertical convergence without any canopy rotation would also increase the included angle between the canopy and caving shield and cause an increase in retract-side pressure.

KINEMATICS OF SHIELD SUPPORT STRUCTURE

Resolution of the load-carrying capacity of the shield design requires examination of the kinematics of the support structure to assess resultant loading; shield capacity cannot be determined simply from the summation of leg forces alone. Two-dimensional rigid body static analysis of the shield structure is kinematically indeterminant by fourth degree, since there are 14 unknowns but only 10 independent equations derivable from the requirements of static equilibrium.

A generalized schematic of a two-leg shield is shown in figure 11, with the unknown quantities defined as follows:

L = leg force.

N = canopy capsule force.

H_1 = horizontal load acting on the canopy.

H_2 = horizontal load acting on the base.

V_1 = vertical resultant load acting on the canopy.

V_2 = vertical resultant load acting on the base.

LOC 1 = location of resultant vertical load on canopy.

LOC 2 = location of resultant vertical load on base.

G_x = horizontal component of resultant gob load acting on caving shield.

G_y = vertical component of resultant gob load acting on caving shield.

X_g, Y_g = spatial coordinates defining location of resultant gob load.

C = compression lemniscate link force.

T = tension lemniscate link force.

P_x = horizontal reaction at canopy hinge pin (fig. 12).

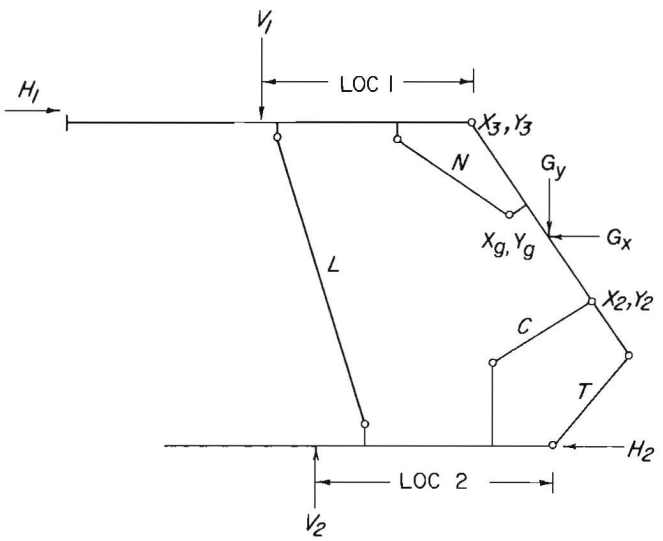

FIGURE 11. - Generalized schematic of two-leg shield.

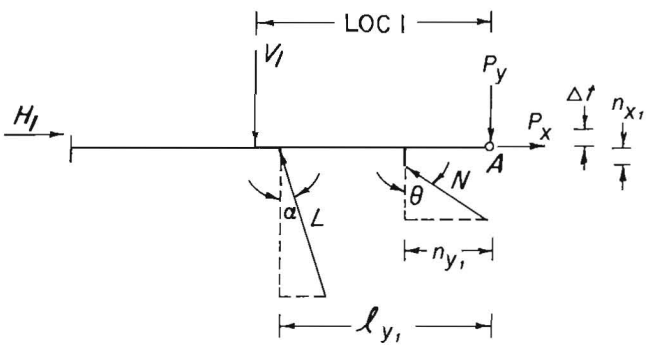

FIGURE 12. - Free-body diagram of forces acting on shield canopy.

P_y = vertical reaction at canopy hinge pin (fig. 12).

The equations of static equilibrium are derived as follows: First, by examination of the forces acting on the canopy, the following three equations are found (fig. 12):

Summation of forces in x direction

$$\Sigma F(x) \rightarrow + = 0$$

$$H_1 - L*SIN\ \alpha - N*SIN\ \theta + P_x = 0 \quad (7)$$

Summation of forces in y direction

$$\Sigma F(y) \uparrow + = 0$$

$$-V_1 + L*COS\ \alpha + N*COS\ \theta - P_y = 0 \quad (8)$$

Summation of moments about point A

$$\Sigma M(A) \curvearrowleft + = 0$$

$$H_1(\Delta t) - V_1(LOC\ 1) + L*COS\ \alpha\ (\ell_{y1}) + N*COS\ \theta\ (n_{y1}) + N*SIN\ \theta\ (n_{x1}) = 0 \quad (9)$$

Examination of the free-body diagram for the canopy-caving shield combination (fig. 13) produces the following equilibrium equations:

Summation of forces in the x direction

$$\Sigma F(x) \rightarrow + = 0$$

$$H_1 - L*SIN\ \alpha - G_x - C_x + T_x = 0 \quad (10)$$

Summation of forces in the y direction

$$\Sigma F(y) \uparrow + = 0$$

$$-V_1 + L*COS\ \alpha - G_y - C_y + T_y = 0 \quad (11)$$

Summation of moments about instantaneous center of lemniscate links (I)

$$\Sigma M(I) \curvearrowleft + = 0$$

$$H_1(c+\Delta t) - V_1(\ell_2) + L*COS\ \alpha\ (\ell_{y2}) - L*SIN\ \alpha\ (c) - G_y(g_y) + G_x(g_x) = 0 \quad (12)$$

Looking at the forces acting on the shield structure as a whole, the following equations can be derived in reference to figure 14.

Summation of forces in the x direction

$$\Sigma F(x) \rightarrow + = 0$$

$$H_1 - G_x - H_2 = 0 \quad (13)$$

Summation of forces in the y direction

$$\Sigma F(y) \uparrow + = 0$$

$$-V_1 - G_y + V_2 = 0 \quad (14)$$

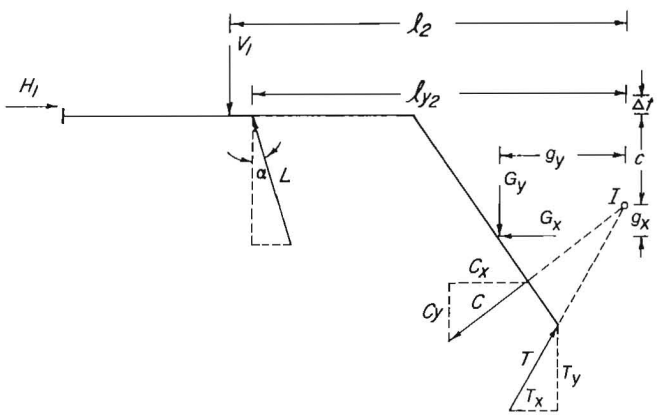

FIGURE 13. - Free-body diagram of forces acting on canopy-caving shield combination.

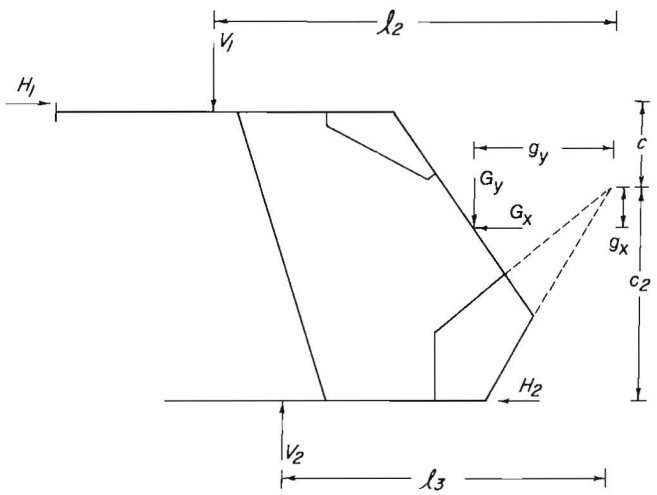

FIGURE 14. - Free-body diagram of forces acting on entire shield.

Summation of moments about instantaneous center of lemniscate links

$$\Sigma M(I) \curvearrowright + = 0$$

$$H_1(c) - V_1(\ell_2) - G_y(g_y) + G_x(g_x) + H_2(c_2) + V_2(\ell_3) = 0 \quad (15)$$

Examination of the free-body diagram for the base (fig. 15) produces the following equations:

Summation of forces in the x direction

$$\Sigma F(x) \rightarrow + = 0$$

$$L*SIN\ \alpha - C_x + T_x - H_2 = 0 \quad (16)$$

Summation of forces in the y direction

$$\Sigma F(y) \uparrow + = 0$$

$$V_2 - L*COS\ \alpha - C_y + T_y = 0 \quad (17)$$

Summation of moments about I

$$\Sigma M(I) \curvearrowright + = 0$$

$$V_2(v_b) - L*COS\ \alpha\ (\ell_b) - L*SIN\ \alpha\ (c_2) + H_2(c_2) = 0 \quad (18)$$

A final equation can be derived from the geometrical requirements that X and Y coordinates are dependent for any part of the shield structure. Referring to figure 11, making reference to the spatial coordinates assigned to the designated hinge points, (X_2, Y_2) and (X_3, Y_3), the unknown coordinates of the location of the resultant gob load can be defined as follows:

$$Y_g = m * X_g + b,$$

where m = slope,

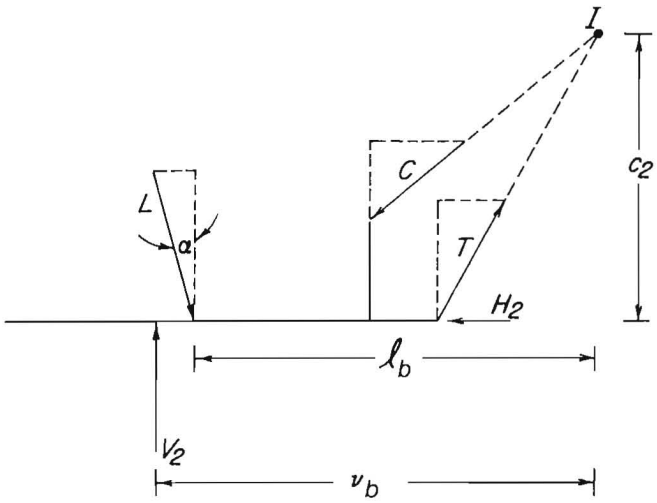

FIGURE 15. - Free-body diagram of forces acting on base.

b = y-intercept,

and X_g, Y_g = coordinates of resultant gob force on caving shield.

Geometrically speaking, the slope is defined as the change in y-direction (rise) divided by the change in the x-direction (run). Hence, the slope is defined as $(Y_3 - Y_2) / (X_3 - X_2)$ and

$$Y_g = \frac{(Y_3 - Y_2)}{(X_3 - X_2)} X_g + \frac{Y_2X_3 - X_2Y_3}{X_3 - X_2}. \quad (19)$$

To solve the foregoing equations, four quantities must be measured. One such method is to determine the vertical resultant and its position on the canopy and base (quantities V_1, V_2, LOC 1 and LOC 2) by measurement of the canopy and base pressure distributions (5). These quantities are measured by load cells placed on the canopy and under the base to measure canopy and base pressure distributions. Once these quantities are known, the remaining unknown parameters can be derived as follows:

1. Horizontal force acting on canopy H_1

Solve equation 9 for H_1.

$$H_1 = \frac{V_1\,(LOC\ 1) - L^*COS\ \alpha\ (\ell_{y1}) - N^*COS\ \theta\ (n_{y1}) - N^*SIN\ \theta\ (n_{x1})}{\Delta t} \tag{20}$$

2. Horizontal force acting on base H_2

Solve equation 18 for H_2.

$$H_2 = \frac{V_2(v_b) + L^*COS\ \alpha\ (\ell_b) + L^*SIN\ \alpha\ (c_2)}{c_2} \tag{21}$$

3. Horizontal component of gob load G_x

Solve equation 13 for G_x.

$$G_x = H_1 - H_2 \tag{22}$$

4. Vertical component of gob load G_y

Solve equation 14 for G_y.

$$G_y = V_2 - V_1 \tag{23}$$

5. Horizontal reaction at canopy hinge P_x

Substitute H_1 into equation 7 and solve for P_x.

$$P_x = \frac{-V_1(LOC\ 1) + L^*COS\ \alpha\ \ (\ell_{y1}) + N^*COS\ \theta\ (n_{y1}) + N^*SIN\ \theta\ (n_{x1})}{\Delta t}$$

$$+ L^*SIN\ \alpha + N^*SIN\ \theta \tag{24}$$

6. Vertical reaction at canopy hinge P_y

Solve equation 9 for P_y.

$$P_y = V_1 + L^*COS\ \alpha + N^*COS\ \theta \tag{25}$$

7. Location of resultant gob load vector (x component) X_g

Solve equation 12 for G_x.

$$g_x = \frac{-H_1(c+\Delta t) + V_1(\ell_2) - L^*COS\ \alpha\ (\ell_{y2}) + L^*SIN\ \alpha\ (c) + G_y(g_y)}{G_x} \tag{26}$$

From equation 19, form g_x and g_y and substitute into equation 26 and solve X_g.

$g_y = X_I - X_g$,

where X_I = x-coordinate of instantaneous center of lemniscate links

and X_g = x-coordinate of resultant gob load.

$g_x = Y_I - Y_g$,

where Y_I = y-coordinate of instantaneous center of lemniscate links

and Y_g = y-coordinate or resultant gob load.

$$X_g = \frac{-H_1(c+\Delta t) + V_1(\ell_2) - L*COS\ \alpha\ (\ell_{y2}) + L*SIN\ \alpha\ (c) + G_x \frac{Y_2X_3 - X_2Y_3}{X_3 - X_2} - G_xY_I}{G_y - G_x \frac{Y_3 - Y_2}{X_3 - X_2}} \quad (27)$$

8. Location of resultant gob load vector (y-component) Y_g.

Substitute X_g into equation 19.

$$Y_g = \frac{Y_3 - Y_2}{X_3 - X_2} X_g + \frac{Y_2X_3 - X_2Y_3}{X_3 - X_2}. \quad (28)$$

RESULTANT LOAD VECTOR THEORY

The problem with the technique provided in the previous section is that the required four known variables (vertical resultant, and location on canopy and base) are extremely difficult to measure. The technique of utilizing load cells on the canopy and under the base to measure associated pressure distributions is questionable for the following reasons:

1. The strata are not uniformly distributed on the canopy-base, and the load cell can disturb this distribution.
2. Only discrete portions of the canopy-base are measured with the load cell providing only a very gross approximation to the pressure distribution.
3. Placement and maintenance of the load cells are difficult (particularly under the base) and must be done with each shield advance.

Assuming there is no gob loading, it is possible to determine the resultant load vector by another technique. A static rigid body analysis of the shield structure reveals that the resultant load vector parameters (magnitude, location, and angle), as shown in figure 1, can be determined from the following resultant load vector parameter equations if the leg, canopy capsule, and compression lemniscate link forces are known.

RESULTANT LOAD VECTOR PARAMETER EQUATIONS

$$HORZ = 0.2426 * L + 0.0192 * N + 0.3765 * C,$$

$$VERT = 0.9699 * L - 0.0997 * N + 0.0038 * C,$$

$$MAG = (HORZ^2 + VERT^2)^{1/2},$$

$$LOC = \frac{28.2524 * L + 9.4515 * N}{VERT},$$

$$ANG = ARCTAN\ (VERT/HORZ),$$

where HORZ = horizontal component of resultant magnitude, ton,

VERT = vertical component of resultant magnitude, ton,

MAG = resultant magnitude, ton,

LOC = resultant location, inches from canopy hinge,

ANG = resultant angle, degrees,

L = average leg force, ton,

N = net canopy capsule force, ton,

C = average compression lemniscate link axial force, ton.

The foregoing equations present the relationships developed for a two-leg, 360-ton shield when used in a 94-in-high configuration. These are not general relationships; rather, they represent the shield and associated geometry currently under field study by the Bureau. Similar equations, with different coefficients, will result for other geometries and other shields.

The vector parameter equations are derived from three independent equations produced by summation of moments about the canopy hinge pin (equation 29 and figure 16), the instantaneous center of the lemniscate links (equation 30 and figure 17), and the tension link-caving shield hinge pin (equation 31 and figure 18).

$$-VERT*LOC + L*COS(14.10)*29.13 + N*SIN(31.22)*4.92 + COS(31.22)*8.07 = 0 \quad (29)$$

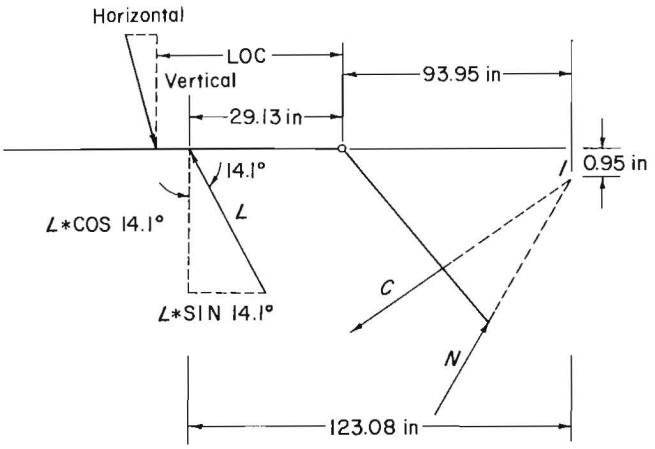

FIGURE 17. - Summation of moments acting at instantaneous link center; see equation 30.

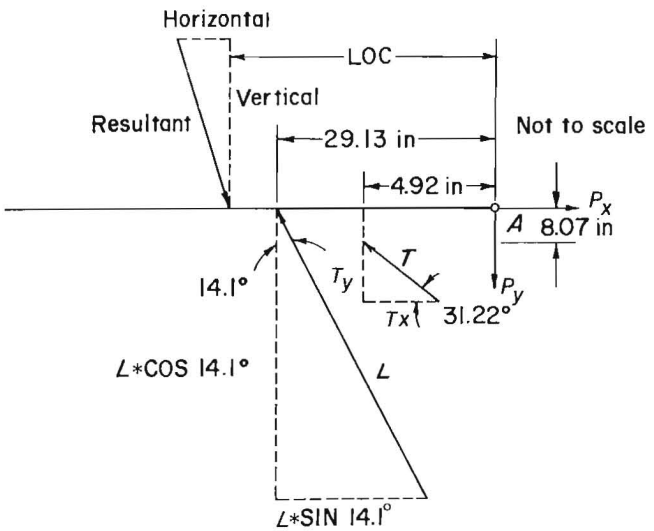

FIGURE 16. - Summation of moments acting at canopy hinge; see equation 29.

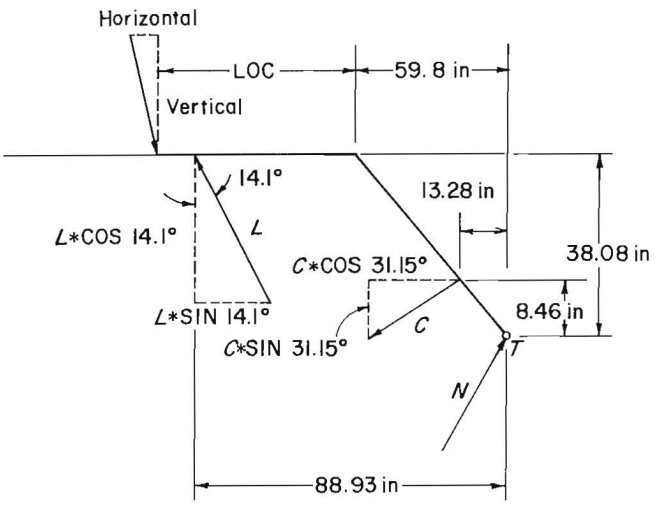

FIGURE 18. - Summation of moments acting at tension link pin; see equation 31.

$$-VERT*(LOC+93.95) + HORZ*0.95 + L*COS(14.10)*123.08 - L*SIN(14.10)*0.95 = 0 \quad (30)$$

$$-VERT*(LOC+59.80) + HORZ*38.08 + L*COS(14.10)*88.93 - L*SIN(14.10)*38.08$$
$$-C*COS(31.15)*8.46 - C*SIN(31.15)*13.28 = 0 \quad (31)$$

DERIVATION OF VECTOR EQUATIONS

Step 1: Solve equation 30 for HORZ.

$$HORZ = 1.0526\ VERT(LOC) + 98.8947\ VERT - 129.5579\ L*COS(14.10) + L*SIN(14.10).$$

Step 2: Solve equation 29 for VERT(LOC).

$$VERT(LOC) = 29.13\ L*COS(14.10) + 4.92\ N*SIN(31.22) + 8.07\ N*COS(31.22).$$

Step 3: Substitute VERT(LOC) from step 2 and HORZ from step 1 into equation 31 and solve equation 31 for VERT.

$$VERT = L*COS(14.10) - 0.0519\ N*SIN(31.22) + 0.0851\ N*COS(31.22)$$
$$+ 0.0023\ C*COS(31.15) + 0.0036\ C*SIN(31.15).$$

Step 4: Substitute VERT(LOC) from step 2 and VERT from step 3 into equation 29 to determine HORZ.

$$HORZ = -0.0010\ L*COS(14.10) + 0.0462\ N*SIN(31.22) + 0.0786\ N*COS(31.22)$$
$$+ 0.2257\ C*COS(31.15) + 0.3544\ C*SIN(31.15) + L*SIN(14.10).$$

Step 5: Solve equation from step 2 for LOC.

$$LOC = \frac{29.12\ L*COS(14.10) + 4.92\ N*SIN(31.22) + 8.07\ N*COS(31.22)}{VERT}.$$

Step 6: By geometry, resultant angle equals arc tangent of HORZ/VERT.

$$ANG = ARCTAN\ (HORZ/VERT).$$

A sensitivity study was conducted to show the effect of a 5-pct change in each of the input variables (leg pressure, capsule pressure, and link strain) on the resultant load vector parameters with each variable studied separately. The results are shown in table 1 for a hypothetical case consisting of a resultant

TABLE 1. - Resultant load vector parametric sensitivity analysis

(Δ vector parameters, pct)

Vector parameters	5-pct Δ leg pressure	5-pct Δ capsule pressure	5-pct Δ link strain
Resultant magnitude.....	5.04	0.04	0.08
Resultant angle.....	.47	.02	.48
Resultant location.....	.18	.19	.00
Horizontal force.....	12.44	.36	7.08
Vertical force.....	4.97	.04	.08

magnitude of 302.71 tons, location of 28.16 in, and angle of 84.30°, which correspond to a vertical load of 301.21 tons and a horizontal load of 30.06 tons. Examination of the data reveals the degree of correlation between input and vector parameters. Of the three vector parameters, magnitude is most dependent upon a single variable (i.e., leg pressure), showing the largest impact by the 5-pct sensitivity analysis. Leg pressure is dominant in all three vector parameters, but resultant location is strongly correlated to canopy capsule pressure, and resultant angle and horizontal force show a strong dependence on link strain.

The above sensitivity analysis is for a specific case of a 5-pct change in each input variable. More generally, the sensitivity of the vector parameters to input variables can be expressed mathematically in terms of partial derivatives of the vector equations as follows:

$$VF = a_1(L) + a_2(N) + a_3(C), \quad (32)$$

$$\Delta VF = \frac{\partial VF}{\partial L} \Delta L + \frac{\partial VF}{\partial N} \Delta N + \frac{\partial VF}{\partial C} \partial C, \quad (33)$$

where VF = any of the vector parameter equations (HORZ, VERT, MAG, LOC, ANG),

and L, N, C = input variables (leg pressure, capsule pressure, link strain).

Examination of the coefficients produced by the partial derivatives will indicate the relative sensitivity of the input variables. Equations for ΔVERT and ΔHORZ are shown below as examples, with the dominant coefficients highlighted. Equations for ΔLOC, ΔANG, and ΔMAG are not easily simplified and hence are not shown.

$$\Delta HORZ = 0.243 * L + 0.091 * N + \underline{0.276} * C$$

$$\Delta VERT = \underline{0.970} * L - 0.100 * N + 0.004 * C$$

The assumptions made in these studies of the resultant load vector concept were primarily twofold:

1. A planar (two-dimensional) static model was utilized as opposed to a three-dimensional model.

2. There was assumed to be no gob (caving shield) loading.

Because the model was planar static, all parameters were measured with respect to a plane defined by the vertical (roof-to-floor) and horizontal (face-to-waste) axes. The lateral dimension (parallel to the face line) was not considered in this two-dimensional model. The three-dimensional shield then becomes simply a two-dimensional "stick" model. The lack of a three-dimensional model prevents determination of lateral position (across the canopy width) or lateral inclination (parallel to the face line) of the resultant load vector. Hence loading parallel to the face cannot be determined from this model.

A preliminary theoretical analysis of the effect of gob loading was made for the specific shield geometry under study. Table 2 presents results for a gob load applied at the gob (caving) shield center with angles up to 45° from vertical and magnitudes up to 50 tons (fig. 19). The table shows relative deviations in the vector parameters, expressed both as measured differences and as percent difference. The base case utilized for the gob study was 29.79 tons of horizontal force and 301.21 tons of vertical force, producing a resultant magnitude of 302.68 tons, an angle of 84.35°, and a location of 28.16 in. Examination of the data reveals that gob load has the largest

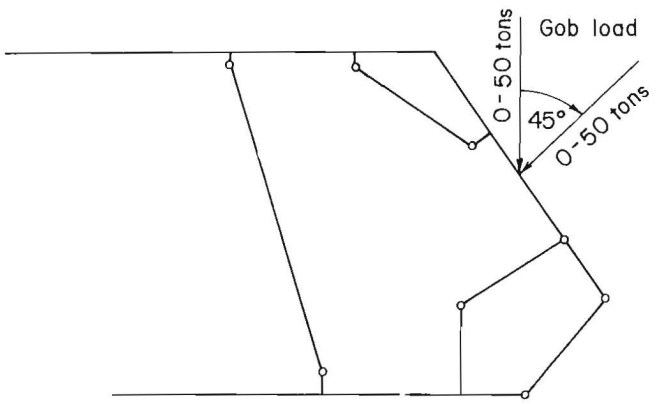

FIGURE 19. - Static analysis of gob load.

TABLE 2. - Impact of gob load on resultant load vector parameters

Load at angle of---	Δ horizontal force		Δ vertical force		Δ resultant magnitude		Δ resultant angle		Δ resultant location	
	tons	pct	tons	pct	tons	pct	deg	pct	in	pct
GOB LOAD = 10 TONS										
15°	2.31	7.75	7.11	2.36	7.30	2.41	0.31	0.37	0.68	2.42
30°	1.52	5.12	6.88	2.29	7.00	2.31	.16	.19	.66	2.34
45°	.64	2.14	6.19	2.06	6.22	2.06	.00	.01	.59	2.10
GOB LOAD = 30 TONS										
15°	6.92	23.24	21.32	7.08	21.86	7.22	0.98	1.16	2.15	7.62
30°	4.57	15.35	20.65	6.86	20.99	6.93	.51	.61	2.07	7.36
45°	1.91	6.42	18.57	6.17	18.67	6.17	.01	.02	1.85	6.57
GOB LOAD = 50 TONS										
15°	11.54	38.74	35.54	11.80	36.38	12.02	1.72	2.04	3.77	13.38
30°	7.62	25.59	34.42	11.43	34.97	11.55	.90	1.07	3.63	12.90
45°	3.19	10.69	30.95	10.28	31.11	10.28	.03	.03	3.22	11.45

TABLE 3. - Impact of support height on resultant load vector parameters

Support height, in	Magnitude, tons	Location, in	Angle, deg	Horizontal force, tons	Vertical force, tons
100.51	341.30	30.07	97.16	42.55	338.64
97.49	341.41	30.07	97.27	43.21	338.67
94.30	341.56	30.07	97.37	43.82	338.73
90.91	341.74	30.07	97.45	44.28	338.86
87.29	341.96	30.06	97.52	44.73	339.03

impact on the horizontal force prediction. The magnitude of error decreases as the gob load vector inclination moves away from vertical and increases with increasing gob load. In the worst case examined, the magnitude of the horizontal load error was -11.54 tons, which would not prevent the Bureau from achieving its goal of determining a first-order approximation of underground horizontal loading. The net result in the prediction of the resultant angle due to the presence of gob load is relatively insignificant, since the vertical loading decreased proportionally to the decrease in horizontal load. The effect of gob load on resultant location is to move the position of the resultant load vector forward and, in the case examined, cause a reduction in support resistance of up to 37 tons, as shown by the deviation in the resultant magnitude.

A sensitivity analysis was also conducted to show the impact of support height on resultant load vector determinations. For the two-leg, 360-ton shield under study, support height was varied over a 12-in range with the midpoint set at the current operating height of 94 in. At this operating height, the variation in support height was shown to have relatively little impact on the resultant load vector parameters as shown in table 3. At the upper and lower limits of the shield operating range, the impact of height variation will be more significant.

RESULTANT LOAD VECTOR INSTRUMENTATION AND FORCE CALCULATIONS

The required known variables for the determinaion of the resultant load vector parameters have been defined as leg, canopy capsule, and compression

lemniscate link forces based upon the static analysis of the shield structure, as presented in the previous section. To measure these variables, an eight-sensor transducer array as shown in figure 20 was selected consisting of the following:

1. Two pressure transducers (one in each leg cylinder) to measure leg pressure.
2. Two pressure transducers, one to measure canopy capsule extension and one to measure retraction pressure.
3. Four strain gauges (two on each compression link) to measure lemniscate link strain.

The pressure transducers were rated at 10,000 psi with accuracies of 0.25 pct (canopy capsule) and 1.0 pct (leg cylinders) of full-scale, equaling 25 psi and 100 psi respectively. Figure 21 displays the pressure transducers utilized in this study. The pressure transducers were installed utilizing quick-disconnect hydraulic fittings in the appropriate lines of the canopy capsule and leg cylinder hydraulic circuits. Calculation of the forces from the pressures is achieved by multiplication of the measured pressure by the corresponding area of the cylinder. For the support under study, these areas are indicated in the following computations:

Leg cylinder

$$\text{Force (tons)} = P * 58.921 \text{ in}^2 \times 1 \text{ ton}/2{,}000 \text{ lb} \quad (34)$$

Canopy capsule cylinder

Extend side $$\text{Force (tons)} = P * 22.187 \text{ in}^2 \times 1 \text{ ton}/2{,}000 \text{ lb} \quad (35)$$

Retract side $$\text{Force (tons)} = P * 12.326 \text{ in}^2 \times 1 \text{ ton}/2{,}000 \text{ lb} \quad (36)$$

where P = measured pressure, psi.

Determination of link forces is considerably more difficult and requires an examination of the structural properties of the link. A structural diagram of the compression lemniscate link for the two-leg, 360-ton shield under study is shown in figure 22. As previously indicated, the measured quantities relative to the compression lemniscate link are the strain on the front and rear surface of the link. The required parameter for the static analysis of the shield is the

KEY

LP	Left leg cylinder pressure transducer
RP	Right leg cylinder pressure transducer
CE	Canopy capsule extend pressure transducer
CR	Canopy capsule retract pressure transducer
LTR	Left compression lemniscate link rear face strain gauge
RTR	Right compression lemniscate link rear face strain gauge
LTF	Left compression lemniscate link forward face strain gauge
RTF	Right compression lemniscate link forward face strain gauge

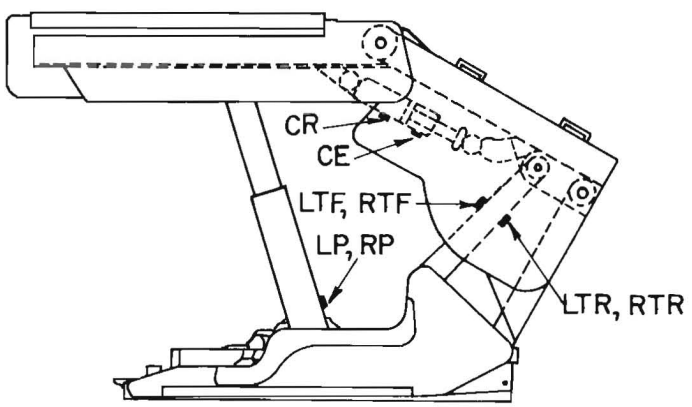

FIGURE 20. - Resultant load vector instrumentation array.

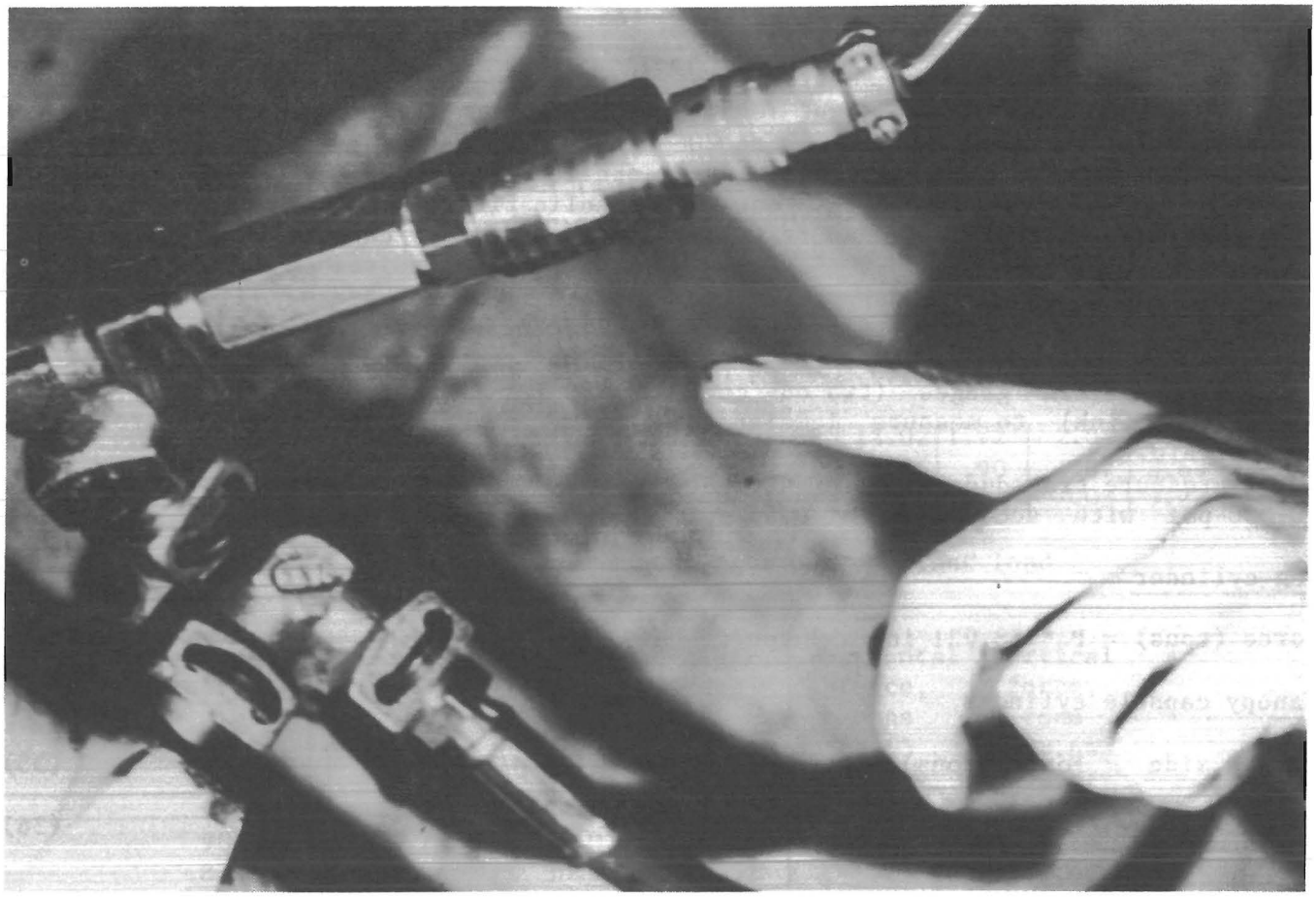

FIGURE 21. - Pressure transducer.

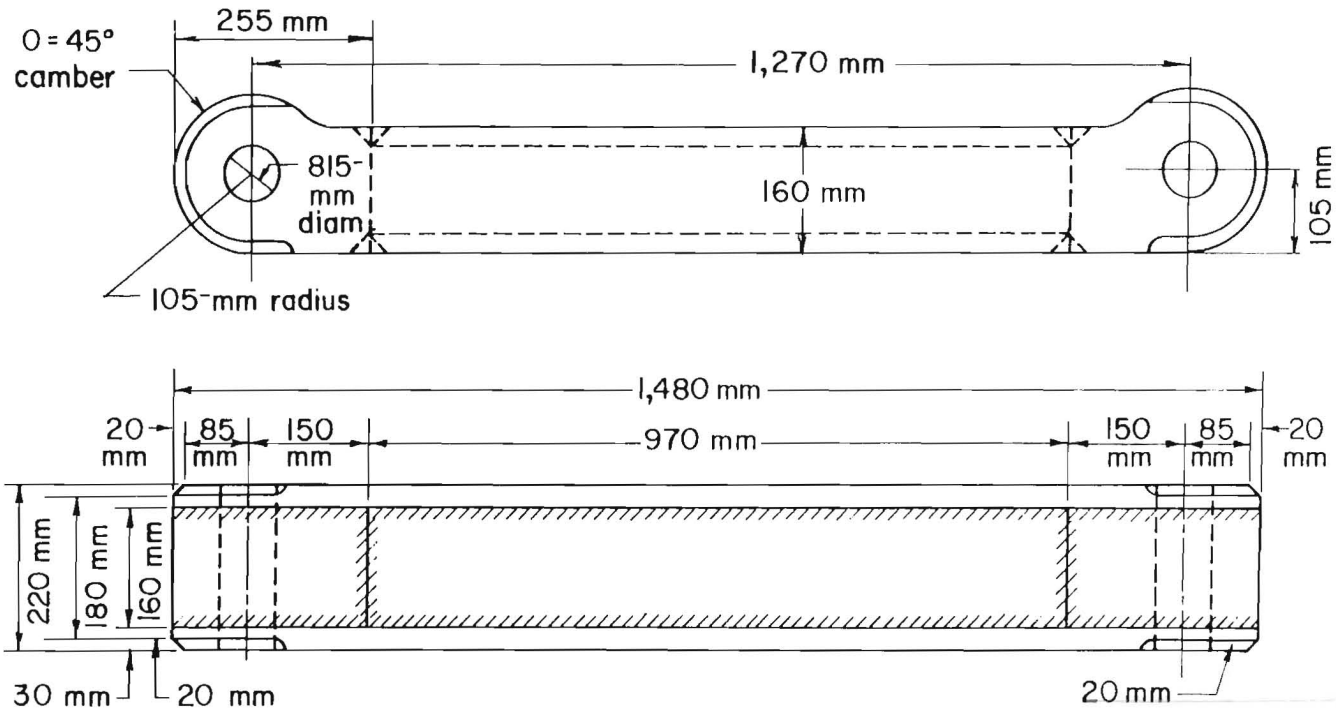

FIGURE 22. - Compression lemniscate link structural diagram.

axial link loading (C), which by definition is the force at the centroid of the member.

In theory, if all the forces acting on the member are known, and if the strain on any fiber in the cross section of the member is measured, the resultant stress at the centroid can be derived if the location of the centroid is known. This would indicate that only one strain gauge would be required to determine axial link force. In practice, however, the link is not subject to simple axial loading, but suffers also from bending stresses caused by pin eccentricity and pin friction. Mathematically, these relationships can be expressed as follows:

$$\text{Resultant stress } (\sigma_r) = \text{axial stress } (\sigma_a) + \text{bending stress } (\sigma_b). \quad (37)$$

It is noticed from figure 22 that the link is essentially C-shaped with the pins offset from the link center. The resultant stress identified in equation 38 is then determined as follows:

$$\sigma_y = \frac{C}{A} + \frac{C*e*y}{I_x}, \quad (38)$$

where σ_y = stress at designated point y in cross section,

C = axial force,

A = cross-sectional area,

e = eccentric moment arm,

y = distance to centroid axis,

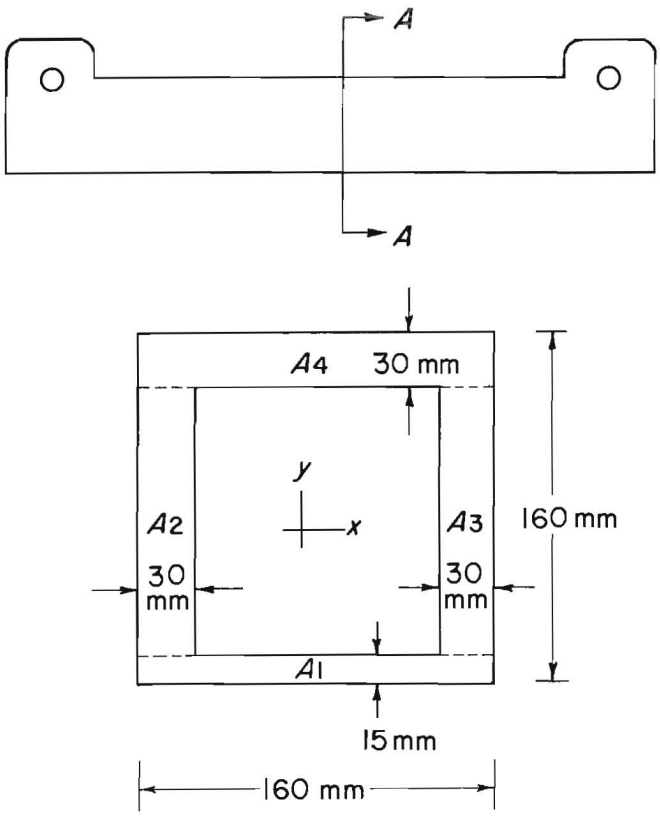

FIGURE 23. - Cross section of compression lemniscate link.

and I_x = moment of inertia.

As can be seen, several unknown quantities must be determined to solve this expression for the resultant stress at a designated point in the link cross section.

A cross section (section A-A) of the link is shown in figure 23. The centroid with respect to the y-axis is found by summation of moments expressed mathematically as follows:

$$\Sigma M(x) = yA = y_1 * \Delta A_1 + y_2 * \Delta A_2 + y_3 * \Delta A_3 + y_4 * \Delta A_4. \quad (39)$$

	Areas	y_1	y
$A_1 = 220 \times 15 =$	3,300	7.5	24,750
$A_2 = 115 \times 30 =$	3,450	72.5	250,125
$A_3 = 115 \times 30 =$	3,450	72.5	250,125
$A_4 = 220 \times 30 =$	6,600	145.0	950,700
	16,800 mm^2		1,482,000 mm

$$y = \frac{\Sigma M(x)}{A} = \frac{1,482,000}{16,800} = 88.21 \text{ mm} = 3.47 \text{ in.} \tag{40}$$

$$\text{Cross-sectional area (A)} = 16,800 \text{ mm}^2 = 26.04 \text{ in}^2. \tag{41}$$

The moment of inertia is found by multiplying each element of area dA by the square of its distance from the x-axis and integrating over the entire section of the member.

$$I_x = \int y^2 \, dA, \tag{42}$$

where I_x = moment of inertia,

y^2 = square of distance from x-axis,

and dA = differential area.

Using the parallel axis theorem, which states that the moment of inertia I_x of an area with respect to any given axis AA' is equal to the moment of inertia I_o with respect to the centroid axis BB', parallel to AA', plus the product Ad^2 of area A and distance d between the two axes, the moment of inertia can be calculated with the equation

$$I_x = I_o + Ad^2. \tag{43}$$

The moment of inertia for the lemniscate link can further be simplified by determining the moment of inertia for the entire cross section as a solid, then subtracting the hollow interior section. Calculations are made as follows:

Entire section

$$I_o = \frac{bh^3}{12} = \frac{(220)\ (160)^3}{12} = 7.51 \times 10^7 \text{ mm}^4 \tag{44}$$

d_1 = distance from center of section to centroid

= 6.3/2 = 3.47 = 0.32 in = 8.21 mm

$Ad_1^2 = (220) \times (160)\ (8.21)^2 = 2.37 \times 10^6 \text{ mm}^4$

$I_o + Ad_1^2 = 7.51 \times 10^7 + 2.37 \times 10^6 = 7.75 \times 10^7 \text{ mm}^4$

Hollow interior

$$I_o = \frac{bh^3}{12} = \frac{(160)\ (115)^3}{12} = 2.03 \times 10^7 \text{ mm}^4 \tag{45}$$

d_2 = distance from center of hollow interior to centroid

= 0.61 in = 15.71 mm

$Ad_2^2 = (160 \times 115)\ (15.71)^2 = 4.54 \times 10^6 \text{ mm}^4$

$I_o = 2.03 \times 10^7 + 4.54 \times 10^6 = 2.48 \times 10^7 \text{ mm}^4$

Moment of inertia I_x

$$I_x = 7.75 \times 10^7 - 2.48 \times 10^7 = 5.27 \times 10^7 \text{ mm}^4 = 126.6 \text{ in}^4 \quad (46)$$

Now, referring to equation 35, the resultant stress at any location in the cross section can be determined from the following relationship:

$$\sigma_i = C \left[\frac{1}{26.04} + \frac{0.66\ (y_i)}{126.6} \right]. \quad (47)$$

Since the measured quantity is strain and not stress, it is also necessary to convert the strain measurements into stress in accordance with the following relationship:

$$\sigma = E * \varepsilon \quad (48)$$

where σ = stress, psi,

E = modulus of elasticity = 30×10^6 for steel, psi,

and ε = strain, microstrain.

Hence, by measurement of the strain with a strain gauge at the top or bottom surface of a link, it would be possible to compute the axial link loading, C.

If these were the only forces acting on the member, the stress ratio of top to bottom should remain constant. This ratio can be computed as 2.62 from equation 45 as follows:

$$\sigma \text{ Top} = C \left[\frac{1}{26.04} + \frac{0.66\ (2.83)}{126.6} \right] = 0.0532\ C$$

$$\sigma \text{ Bottom} = C \left[\frac{1}{26.04} + \frac{0.66\ (-3.47)}{126.6} \right] = 0.0203\ C$$

$$\frac{\sigma \text{ Top}}{\sigma \text{ Bottom}} = \frac{0.0532\ C}{0.0203\ C} = 2.62 \quad (49)$$

Test results, however, revealed that the stress ratio is in excess of the 2.62 value, indicating that other forces were acting on the member. The missing force is the bending moment at the lemniscate link pin connection caused by friction between the pin and link and friction between the link and adjoining member, which produces additional bending stress in the link. Since this quantity is difficult to measure, two strain gauges were used on each link to measure both the front and rear surface strain to resolve the actual bending stresses that occurred in the link. From these strain measurements, and assuming the stress is linearly distributed throughout the link cross section, an equation can be derived from which stress can be computed at the link centroid to determine the axial link loading (C).

$$\varepsilon(y) = m * y + b \quad (50)$$

where $\varepsilon(y)$ = strain as a function of link cross section,

m = slope of line,

b = y-intercept,

$$m = \frac{\text{strain at top surface} - \text{strain at bottom surface}}{\text{cross-section depth}},$$

$$b = \frac{\text{top surface strain} + \text{bottom surface strain}}{2},$$

and $$\varepsilon\ (0.32) = \frac{\varepsilon\ \text{Top} - \varepsilon\ \text{Bot}}{6.3}\ (0.32) + \frac{\varepsilon\ \text{Top} - \varepsilon\ \text{Bot}}{2}. \quad (52)$$

Axial link force is then found by multiplying strain at the centroid by the modulus of elasticity and the cross-sectional area.

$$C = \frac{\varepsilon\ (0.32)\ A^*E}{2{,}000}, \quad (52)$$

where C = axial link loading, tons,

ε (0.32) = computed strain at centroid, microstrain,

A = cross-sectional area, in^2,

E = modulus of elasticity = 30×10^6 psi.

LABORATORY ASSESSMENT OF RESULTANT LOAD VECTOR STUDIES

Utilizing the Bureau's MRS, a thorough evaluation of the resultant load vector concept and capabilities of the data acquisition system was conducted to establish confidence intervals for prediction of resultant load vector parameters. Basically, two types of tests were conducted with the aid of the simulator:

1. Load cell tests - A load cell was placed on the support canopy to act as a known load vector for prediction using the resultant load vector sensor array.
2. Horizontal load tests - A known horizontal and vertical load was applied to the support specimen for prediction from the instrumentation on the support.

LOAD CELL TESTS

These tests were limited to pure vertical loading, and the primary objective was to assess the ability to predict the location and magnitude of the resultant load vector as the angle was held constant at 90°. A total of 16 load cell positions were selected, representing 6 locations along the shield axis and 4 across its width, as shown in figure 24. Results of the tests are shown in table 4. Maximum vector parameter prediction errors were 7.76 pct for magnitude, 5.92 in for location, and 2.75° for resultant angle. It should be noted that these maximum errors occurred at a relatively low shield load (only 196 kips) with the vector located in a fairly unstable region of the support; i.e., several inches forward of the leg center line. If the supports are set properly against the roof, loads of 400 kips or greater can be expected. Deviations more representative of anticipated mine loads are--magnitude, less than 2 to 3 pct; location, less than 2 in; and angle, less than 1°.

To put these figures into perspective, preliminary field data indicate leg pressure variations of 5,000 psi during the mining cycle, which alone would result in variations in the resultant magnitude of about 300 tons. Laboratory tests indicate a stability range in terms of resultant location of 10 in on either side of the leg center line for vertical loading. A vector outside this range would not pass through the support base and would cause instability. As for the resultant angle, a friction coefficient of 0.3 would produce an angle change of 16.7°.

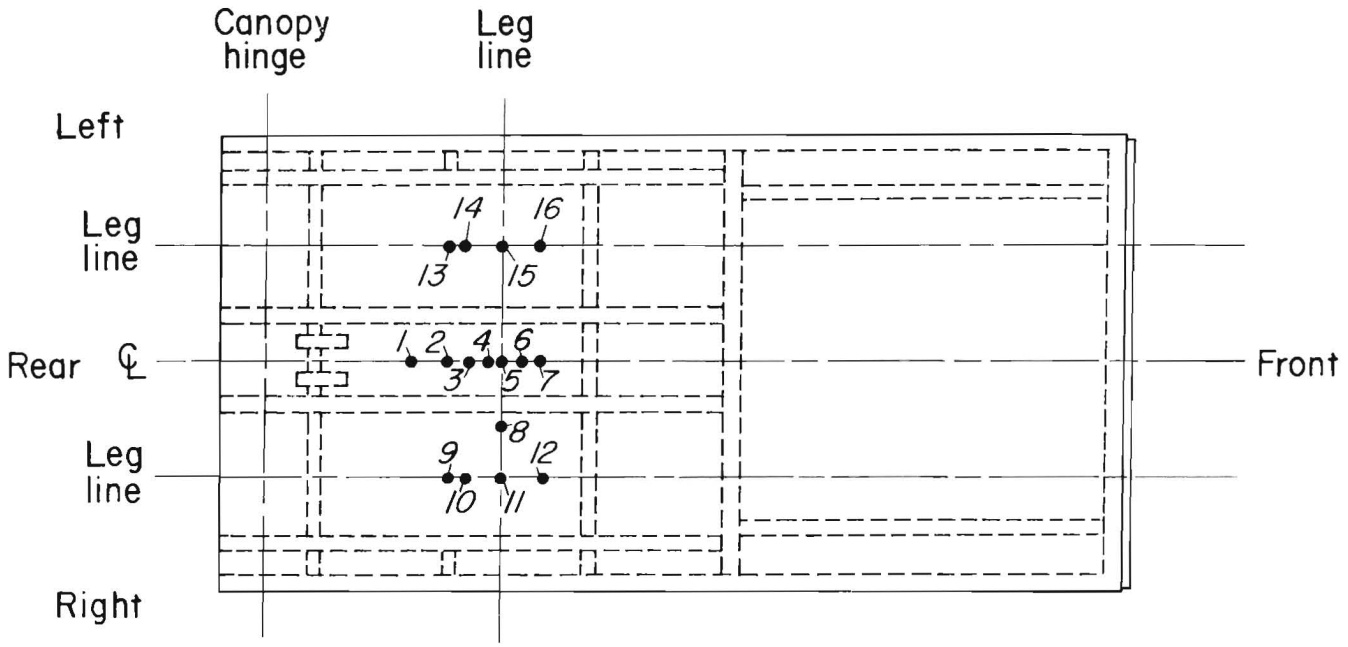

FIGURE 24.- Load cell placement on canopy. (Top view of canopy; 1-16 indicate load cell positions.)

TABLE 4. - Resultant load vector load cell test results

Cell location[1]	AVF,[2] kip	F/AVF,[3] pct	Δ Loc,[4] in	Δ Angle,[5] deg	Cell location[1]	AVF,[2] kip	F/AVF,[3] pct	Δ Loc,[4] in	Δ Angle,[5] deg
1	196	-7.67	5.92	1.39	*10*	236	-6.66	1.69	-1.85
2	210	-5.72	1.69	-.30	*11*	498	-2.85	.05	-.36
3	325	-2.98	.91	-1.52	*12*	481	-2.31	-2.08	.77
4	599	-3.25	.75	-.51	*13*	197	-6.74	1.82	-2.75
5	602	-3.15	-.06	.26	*14*	266	-5.63	1.93	-2.46
6	602	-2.16	-1.09	.55	*15*	512	-3.68	.09	-.58
7	457	-2.83	-2.05	.47	*16*	462	-2.85	-2.06	.63
8	586	-3.39	-.05	.19	Max	NA	-7.67	5.92	-2.75
9	201	-5.80	1.95	-2.03					

NA Not available.
[1]From figure 24.
[2]AVF - measured average vertical force using MRS.
[3]F - array-predicted force magnitude.
[4]Δ Loc - difference between measured and predicted resultant locations.
[5]Δ Angle - difference between measured and predicted resultant angle.

Conclusions drawn from these tests follow:

1. The larger the vertical force applied, the smaller the error in vertical force magnitude.

2. The degree of resultant magnitude error expected at mine load levels is 2 to 3 pct (excluding the gob load disturbance).

3. The magnitude and location prediction deviations are functions of location.

4. All three parameters appear to be independent of location across the width of the canopy, thereby justifying the use of a planar static model for the load conditions analyzed.

HORIZONTAL LOAD TESTS

The objective of these tests was to evaluate the ability of the eight-sensor planar static model and data acquisition hardware to measure horizontal shield loading. The test consisted of preloading the support with a 600-kip vertical force, followed by application of a horizontal load at a rate of 40 kips/min to a maximum of 120 kips; then, using the MRS applied load as the known, the horizontal and vertical forces were predicted from sensors on the support. The test results are shown in table 5. Horizontal load prediction deviations were systematic, with the maximum error of 22.6 kips (11.8 tons) occurring at no horizontal load. The error became smaller, reaching zero at a horizontal load of about 70 kips; then it changed polarity as the load increased to the maximum of 120 kips. Average error in horizontal load prediction was 6.8 kips (3.4 tons). The test results are summarized as follows:

TABLE 5. - Horizontal load prediction test results

Horizontal load, kips		Difference		
Applied	Predicted	pct	kips	tons
0	22.6	NA	22.6	11.8
16	28.8	77.2	12.8	6.4
32	37.0	15.7	5.0	2.5
48	48.4	.9	.4	.2
64	66.0	-1.7	-2.0	-1.0
80	77.8	-2.9	-2.2	-1.1
96	92.0	-4.4	-4.0	-2.0
112	103.6	-7.8	-8.4	-4.2
120	111.8	-6.8	-8.2	-4.1

NA Not available.

1. As a worst case, horizontal load can be measured to within 12 tons. A more optimistic error magnitude would be 5 tons. At the time of these tests, the accuracy of the MRS load application was never fully evaluated, but it is believed to be on the order of 10 tons from preliminary studies. If this is an accurate assessment of the MRS capability, nearly all of the horizontal shield load prediction error could be attributed to MRS resolution error.

2. The lemniscate link is subjected to bending from pin eccentricity and friction and therefore requires a minimum of two gauges per link to assess axial link loading.

3. The dominant variable in determining horizontal load is lemniscate link strain.

4. As horizontal load increases, link strain diminishes, making strain measurements more difficult. Strain values ranged from 78 microstrain at zero horizontal load to 27 microstrain at a 120-kip horizontal load for the rear face gauges, and from 325 to 99 microstrain for the forward link gauges.

FIELD STUDIES

Resultant load vector studies on shield supports were conducted at the Thompson Creek Mine of Snowmass Coal Co. near Carbondale, CO. A layout of the mining plan, depicting the study longwall panel (panel 1) is shown in figure 25. The 360-ft face was operating on a 30° pitch, with approximately one-half of the panel completed at the time of study. The face had been idle for several months prior to the data collection efforts because of poor market conditions in the region. The seam averages about 7.5 ft (2.5 m) in thickness and has an underclay of a competent (Rollins) sandstone and an overlay of a relatively strong interbedded sandstone-shale. The roof caves fairly consistently immediately behind the supports, thereby providing good conditions for longwall mining. A major shear zone cuts diagonally across the final third of the panel, but the effects of the zone were not felt at the face during the data collection efforts.

The powered roof support system utilized at Snowmass is the Hemscheidt Troika system (fig. 26). The supports are two-leg shields rated at 360 tons' capacity. Physical and structural characteristics of the support were provided in the previous sections. The supports are equipped with a 30-in forepole canopy

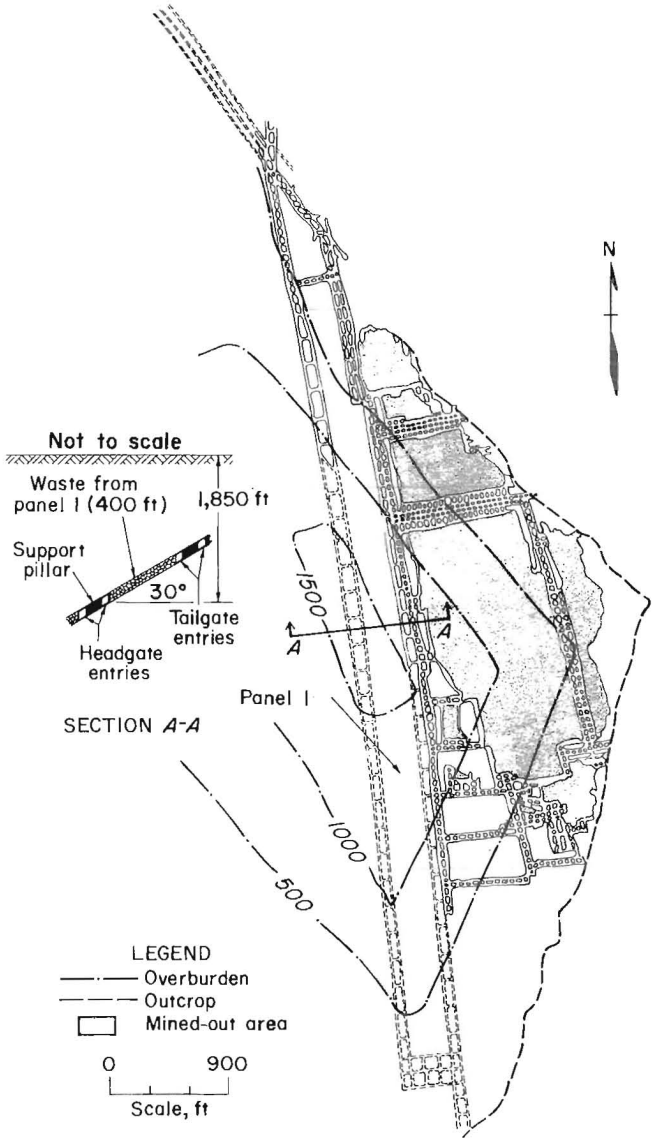

FIGURE 25. - Snowmass Mine longwall layout.

and face spillplates and are designed specifically for steep-seam mining. The supports operate in groups of three and are advanced independent of the face conveyor, which permits self-aligning of the supoprts. The roof support system at Snowmass consisted of 23 Troika sets totaling 69 longwall shields.

DATA ACQUISITION SYSTEMS

Initial efforts to collect resultant load vector field data were largely unsuccessful because of data acquisition instrumentation problems. Two data acqisition systems were utilized for this study because of their availability and prior approval for underground use by the Mine Safety and Health Administration (MSHA). The first system consists of a strain indicator that requires manual intervention to balance the sensor bridge network so that individual sensors could be read. A switching unit is used to switch from channel to channel, and data are manuallly recorded on paper or voice-recorded on magnetic tape. The units are battery powered, intrinsically safe, and approved by MSHA for use at the face. Forty channels of this system were utilized for the underground resultant load vector studies. A strain indicator and switching unit are shown in figure 27.

The second system provides 14 channels of analog data with 8 h of continuous recording onto a magnetic tape recorder. The primary components of the system are the FM tape recorder and the signal conditioning unit, as shown in figure 28, which provide 5-V dc gauge excitation and fixed gains of 500 to 1,000 for signal amplification prior to recording. The system was granted an experimental permit by MSHA for underground use; however, the recorder is not permissible and must be kept in fresh air, requiring coaxial data cables to be strung from each sensor to the recorder. All other components either are intrinsically safe or are placed in explosion-proof boxes. A schematic of the system as it was used underground is shown in figure 29.

The scope of the field effort consisted of instrumenting five longwall shields with the full eight-transducer instrumentation array from which resultant load vector measurements were made. In addition, seven other longwall shields were instrumented with pressure transducers to measure leg pressures only. The arrangement of the instrumented shields on the longwall face is shown in figure 30. A total of 55 shield cycles of data were collected during approximately 75 ft of advance from the instrumented shields, encompassing both data acquisition systems.

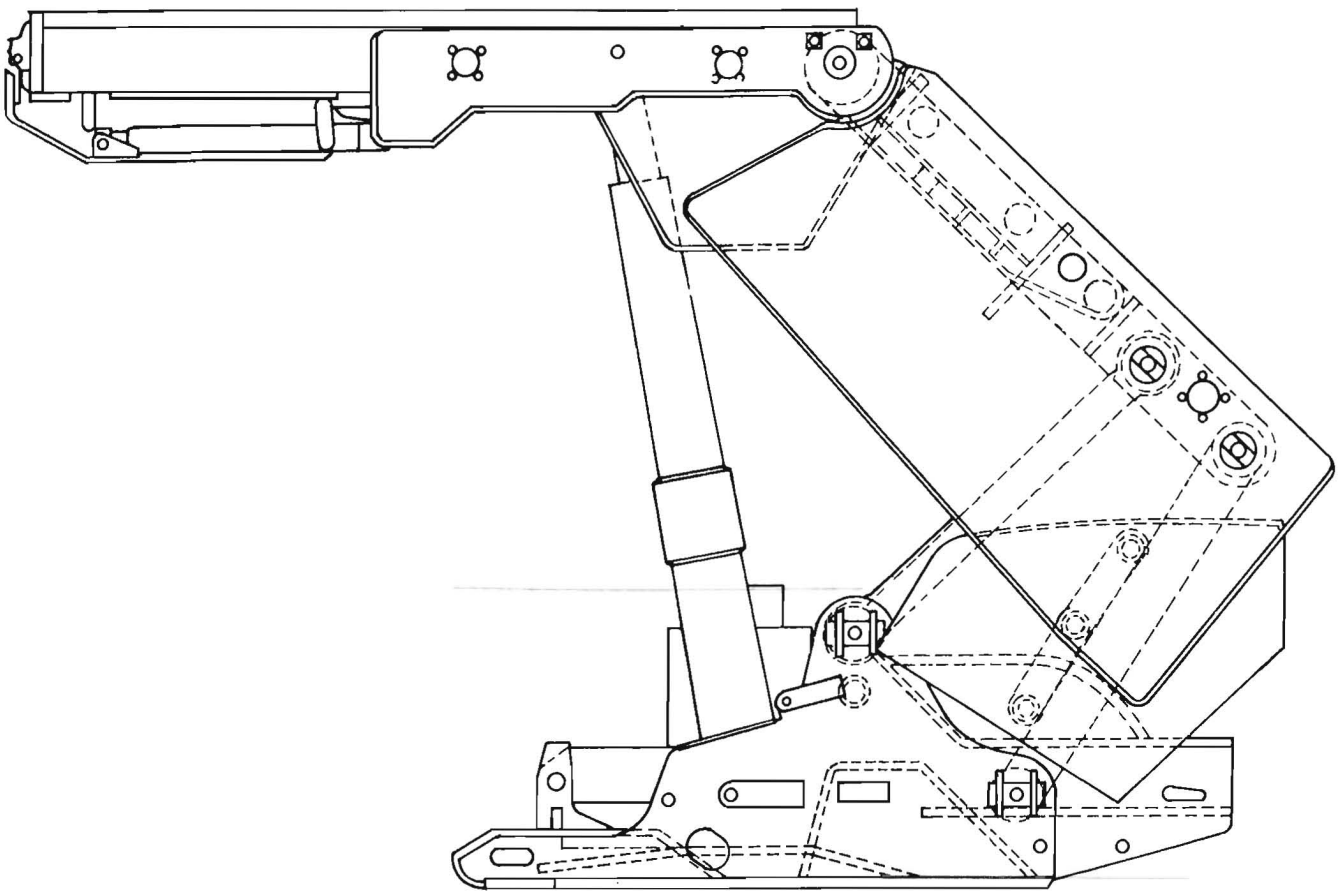

FIGURE 26. - Troika shield.

DATA ANALYSIS

Several interesting observations have been made from the field data, and results appear to be consistent with shield mechanics and anticipated roof behavior. Recalling the static analysis of the shield structure presented earlier, the measured parameters were leg pressure, canopy capsule pressure, and compression lemniscate link strain, from which the resultant load vector parameters of magnitude, location, and direction were determined. A measure of the horizontal and vertical force acting on the support was also calculated from these parameters.

Recalling the discussion on shield mechanics presented earlier, the association between the measured variables and the vector parameters was defined as follows:

Resultant magnitude - leg pressure.

Resultant location - leg pressure and canopy capsule pressure.

Resultant angle - leg pressure and lemniscate link strain.

These associations will be evidenced from the following data presentations. From this analysis, the inadequacies of measuring leg pressures alone, in terms of understanding the behavior of the shield support, become clearly evident, since only the resultant magnitude can be reasonably predicted from leg pressure data alone.

Leg Pressure Data

Leg behavior was found to be very predictable and consistent. A typical leg pressure plot is shown in figure 31. As can be seen from the graph, it is possible to distinguish the passage of the shearer and the adjacent shield activity by the change in the slope of the

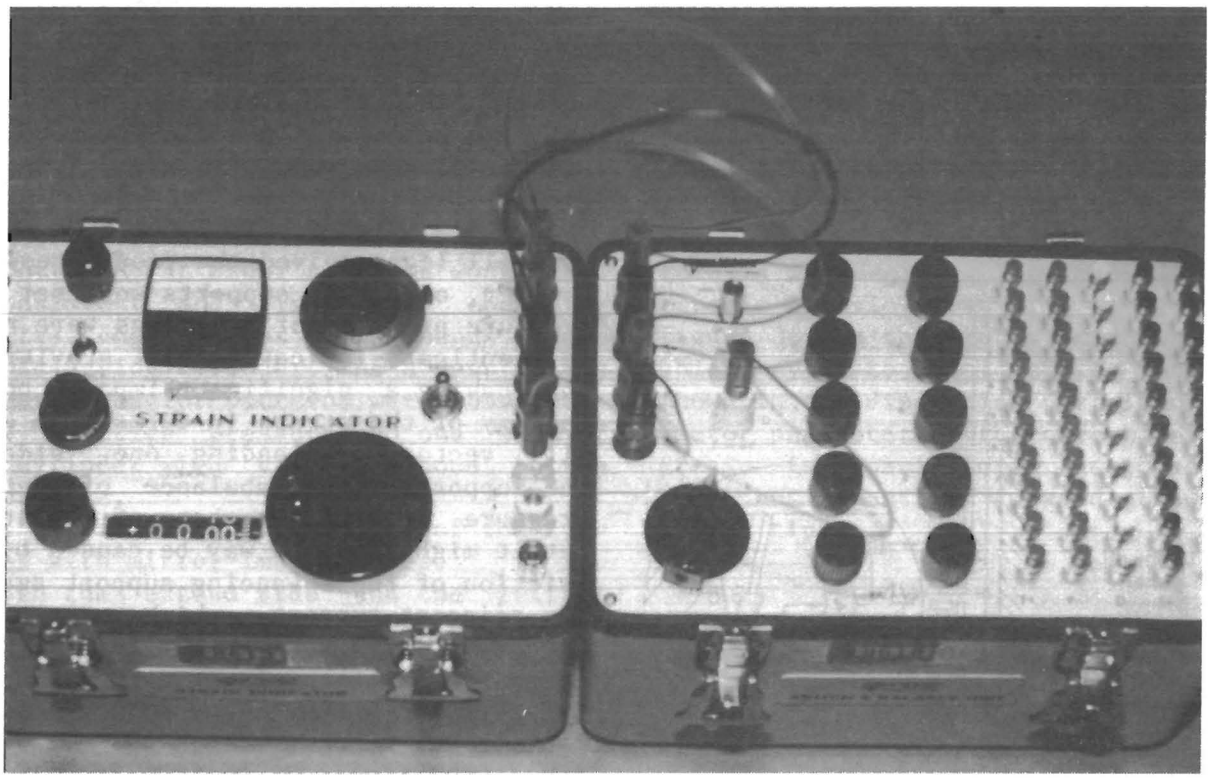

FIGURE 27. - Manual strain indicator and switching unit.

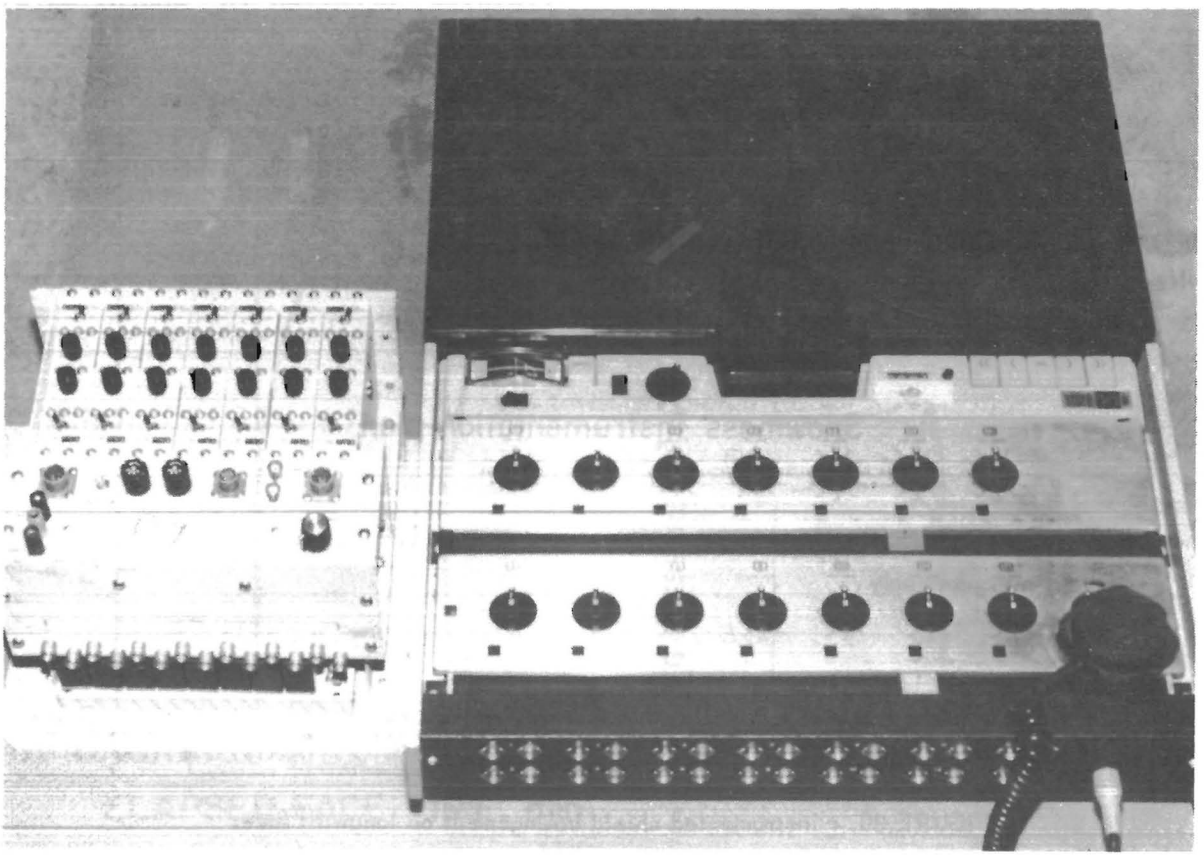

FIGURE 28. - FM tape recorder and signal conditioning unit.

pressure curve. Typically, these events would occur within a relatively small timeframe, so that the effect of both is seen as one pressure rise; however, there are several cases when the events could be individually identified, as in figure 32.

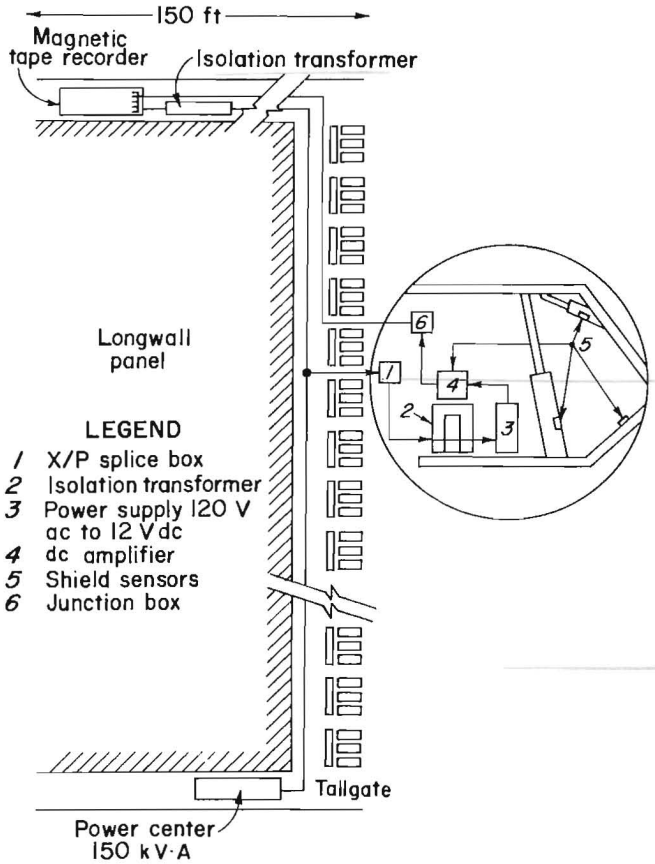

FIGURE 29. - Continuous data acquisition system schematic.

A wide variety of setting pressures were observed with the average of 2,200 psi, well below the rated setting pressure of 4,000 psi. There was also typically an imbalance of leg pressure magnitude between the left and right leg during setting of the support, as depicted in figure 33. Most often the downhill leg received the most pressure. However, once the supports were set, the pressure profiles of both legs were nearly identical, indicating that gravity was not having a significant impact on the geology of the strata in terms of a downhill vector overloading one side of the support. The imbalance of setting pressure remains somewhat of a mystery, but it might in some way be caused by the friction of the advancing support against the adjacent support, which causes it to "bind up" somewhat during setting. Another possible explanation is that the debris left on the canopy during advancement of the support tends to migrate to the downhill side of the support, leaving a partial void for the upper leg to push against during support setting.

Yielding occurred in approximately 25 pct of the monitored shield cycles; however, it must be remembered that the face had been inactive for several months prior to the data collection. Owing to the imbalance in setting pressures between legs, it was common for only one leg to yield. Yield pressure was measured at approximately 6,500 psi.

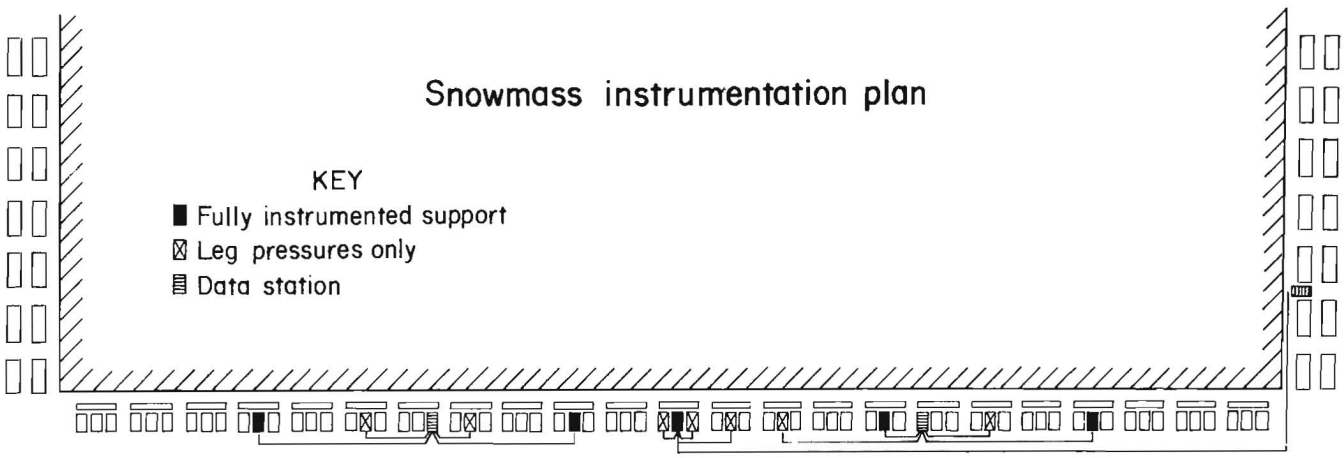

FIGURE 30. - Instrumented shield arrangement on longwall face.

Canopy Capsule Behavior

The canopy capsule behavior was much less consistent and far less predictable than the leg behavior. The behavior tended to be operation oriented, in that sometimes the operator would activate the capsule cylinder during setting of the support, and at other times he would not. Inconsistent and improperly operating (dirty) check valves were found in the double-acting cylinder. As a result, two primary behavior patterns were observed:

1. Positive pressure on one side of the cylinder with virtually none on the other side.
2. Pressure on both sides of the cylinder with mirror-image shapes.

Both the extend side and the retract side were found to be the high-pressure side, as shown in figure 34. Statistically, the extend side was the high-pressure side 58 pct of the time, indicating a load was acting toward the tip of the canopy forward of the leg line. The retract side was found to be the high-pressure side 42 pct of the time, which was indicative of a load to the rear of the leg line. An example of positive pressure on both sides of the cylinder is shown in figure 35, where the extend-side magnitude is shown to be decreasing, while the retract-side magnitude is increasing. The inconsistency in capsule behavior can also be seen from figure 36 as the behavior changes from shield cycle to shield cycle. As will be shown in the discussion pertaining to the vector parameters, the effect of an increase in capsule force is to move the resultant location forward (toward the canopy tip).

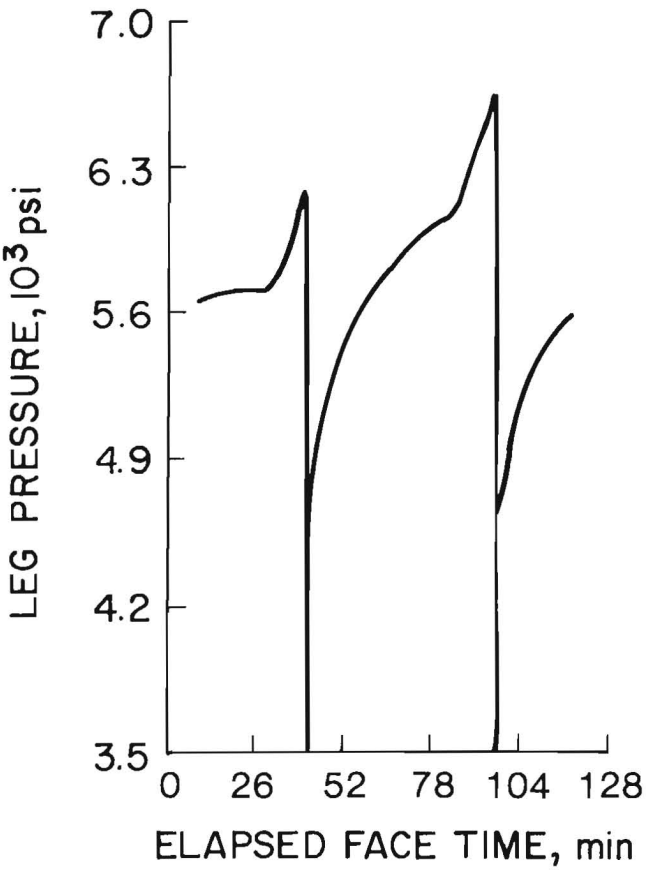

FIGURE 31. - Typical leg pressure plot.

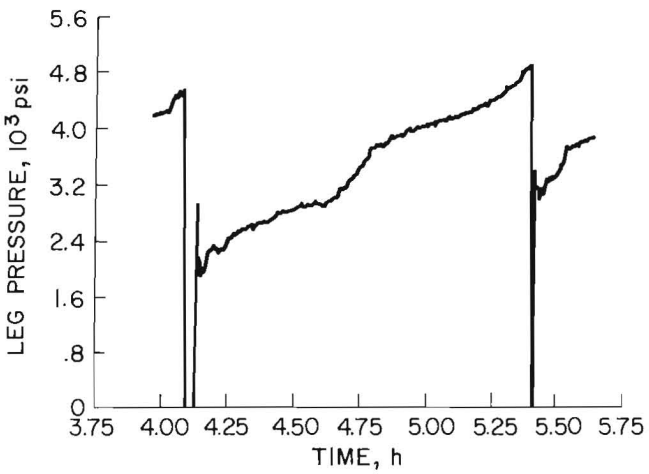

FIGURE 32. - Illustration of shearer move and adjacent shield activity.

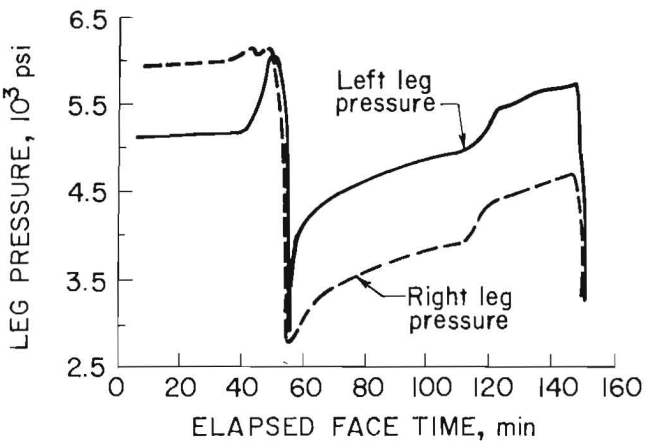

FIGURE 33. - Imbalance of setting pressures on shield supports.

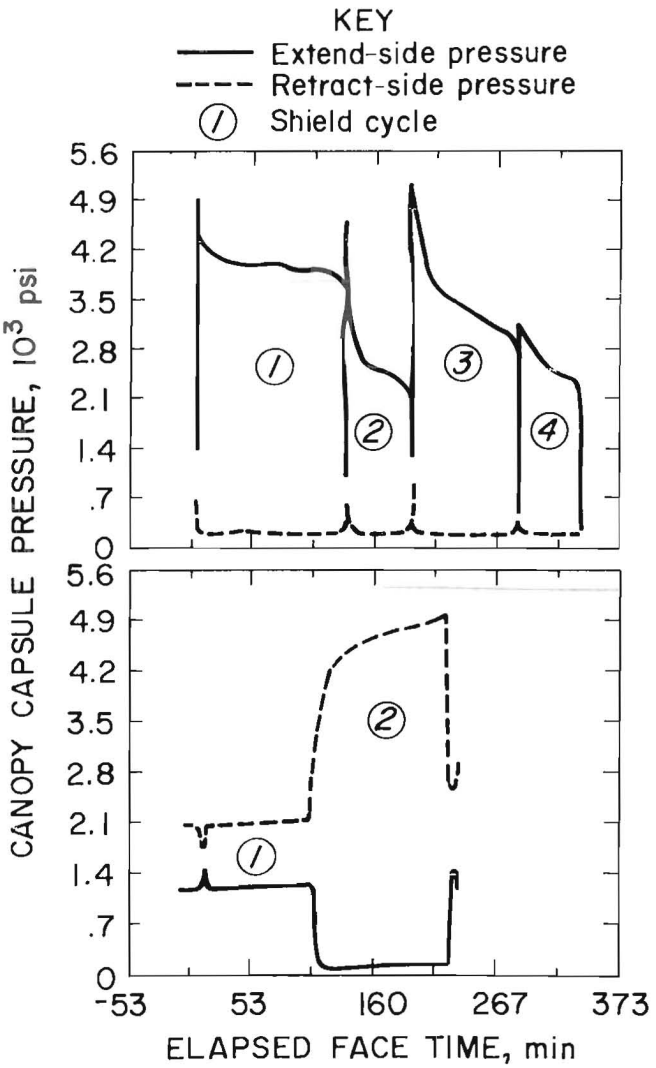

FIGURE 34. - Illustration of extend and retract canopy capsule pressure profiles.

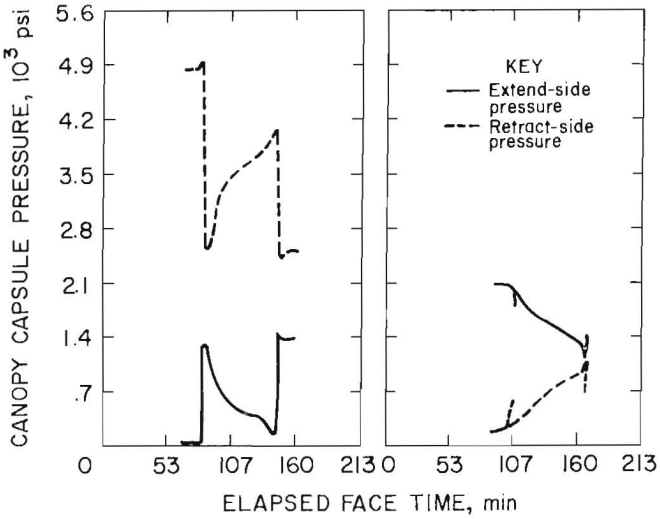

FIGURE 35. - Mirror image capsule pressure behavior.

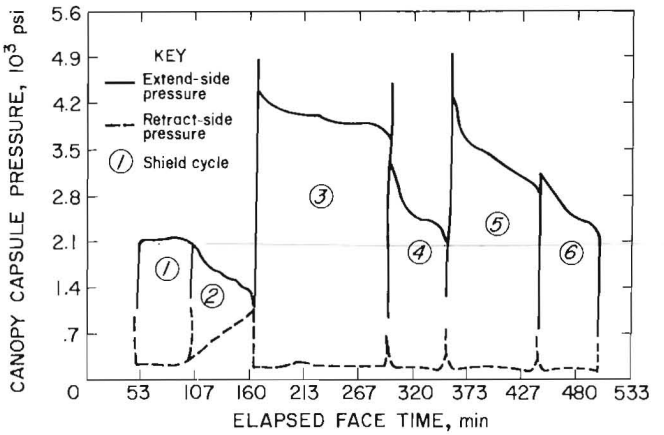

FIGURE 36. - Variation in canopy capsule behavior.

Link Strain Behavior

Recalling the discussion of the functional relationship of the shield components, the forward links in a two-leg shield are intended to be in compression during load application; hence, they are typically called the compression lemniscate links. However, as was observed during the field effort, load cases exist that put the front "compression" link in tension. Three behavior patterns were observed regarding the front link, indicating that several phenomena were occurring. The three observed behavior patterns and their relative frequency of occurrence follow:

1. Both links in compression - 53 pct.
2. One link in tension and one link in compression - 40 pct.
3. Both links in tension - 7 pct.

Figure 37 illustrates cases where both front links were in compression, and cases where one link was in tension while the other was in compression. The graph is interpreted as follows: Sharp changes in magnitude define individual shield cycles owing to the reduction in support loading as the support is lowered and advanced. For the example shown in figure 37, six shield cycles were recorded during this shift. The differential between tension and compression is denoted by the dividing line at zero microstrain. This

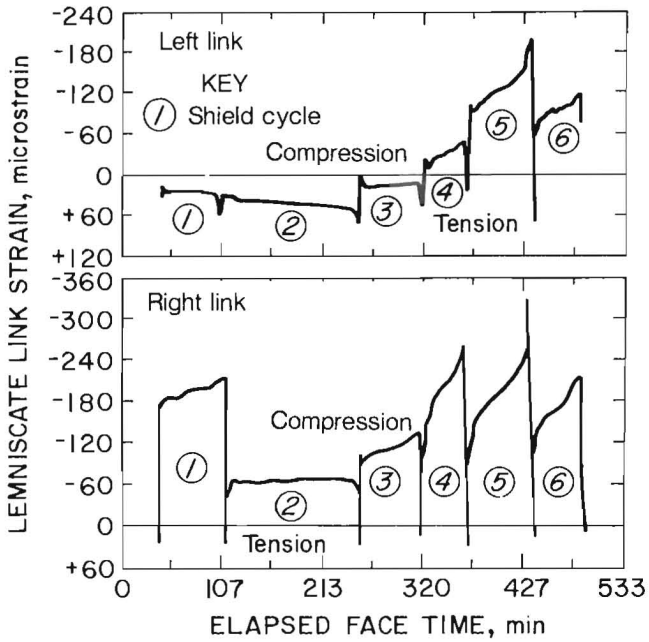

FIGURE 37. - Illustration of strain in compression lemniscate link.

example shows that the right link was in compression while the left link remained in tension for the first three shield cycles; then both links were in compression for the remaining three shield cycles.

Looking at the probable causes of the observed link behavior, as indicated earlier, the expected behavior is for both front links to be in compression during the entire load cycle. As was described in the section on shield behavior, the horizontal component of the leg force causes compression in the forward link, and as the leg pressure increases, the link is further compressed and the strain increases proportionally. Under symmetrical loading conditions, the normal behavior is for both forward links of the shield to be in compression.

The situation in which one link was in tension while the other was in compression probably occurred during advancement of the support, in which there was a rotation of the base relative to the canopy that caused one side of the canopy to be moving toward the gob while the other side was moving toward the face. This rotation of the base relative to the canopy probably was the result of gravity acting on the support owing to the 30°

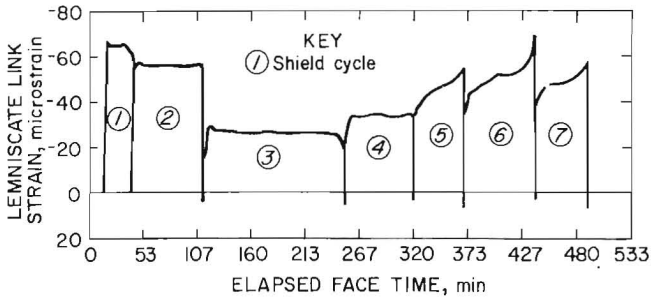

FIGURE 38. - Illustration of constant and increasing link strain.

pitch, as the support tends to bind against the downhill adjacent support during advancement. Another possible explanation for this type of link behavior is unsymmetrical loading, but since the imbalance occurred immediately upon setting of the support with similar strain profiles after set, the previous hypothesis is considered to be more probable.

Again recalling the functional behavior of the shield support presented earlier, horizontal load reduces link loading, and the few cases where both front links were in tension occurred during situations of extremely high horizontal loading. There is some evidence to indicate that particular link strain profiles are operator induced, rather than roof induced. For example, on occasion the operator will "jog" the support back and forth during advancement and/or after setting the support to ensure the support is effectively set against the roof. Since link strain behavior is dependent upon relative motion between the canopy and base, if the operator happens to set the support and then continues to try to advance it with the advance ram, a horizontal force will be induced in the canopy that could cause the abnormal link behavior discussed here with both links in tension.

Generally, two strain profiles were observed: (1) increasing strain during the shield cycle, and (2) fairly constant strain during the shield cycle. Figure 38 illustrates cases of both constant and increasing strain profiles. When the supoprt was subjected to high horizontal loads, cases were observed where the link strain actually decreased during the shield cycle. The strain level varied

significantly from shield cycle to shield cycle, as shown in figure 39, depending on the loading observed, making it difficult to indicate a typical strain magnitude. For the example shown in figure 39, the forward surface gauge strain ranged from a low of about 58 microstrain to a high of 310 microstrain. Changes in strain magnitude during individual shield cycles were also shown to range from a low of 10 microstrain for shield cycle 1, to a high of about 120 microstrain for shield cycle 6. As shown, the rear surface strain is of smaller magnitude (3 to 5 times) because of bending stresses that occurred in the link.

RESULTANT LOAD VECTOR PARAMETERS

The impact of the foregoing variables on the resultant load vector parameters is discussed in the ensuing pages of this report. Emphasis will be placed on the association between the measured variables and the vector parameters, as discussed earlier, and the influence of these parameters on shield mechanics.

Resultant Magnitude

As indicated by the static analysis of the shield structure, the resultant magnitude is strongly dependent upon leg behavior, as the leg force is by far the principal means of support resistance. As can be seen from figure 40, the shape of the resultant magnitude curve is nearly identical to that of the leg pressure plot, illustrating the association between leg force and resultant magnitude. As is the case with leg pressures, the resultant magnitude is influenced by the shearer and adjacent shield activity. The sensitivity of the resultant magnitude to leg behavior is shown in figure 41, where the effect of a yielding leg is clearly represented in the resultant magnitude plot. The resultant magnitude was found to range from 172 to 360 tons and to consistently increase during the shield cycle as the strata converged and caused additional loading on the support. The resultant magnitude was also found to vary significantly from shield cycle to shield cycle, as shown in figure 42, reflecting the variation of setting pressures achieved. However, examination of the change in resultant force from the beginning to the end of the shield cycle reveals similar load profiles and a relatively small variation in support resistance.

$$\Delta R = Rmax - Rmin, \qquad (53)$$

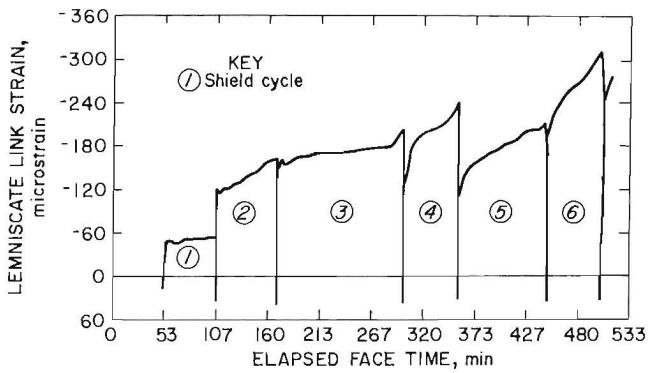

FIGURE 39. - Range of lemniscate link strains.

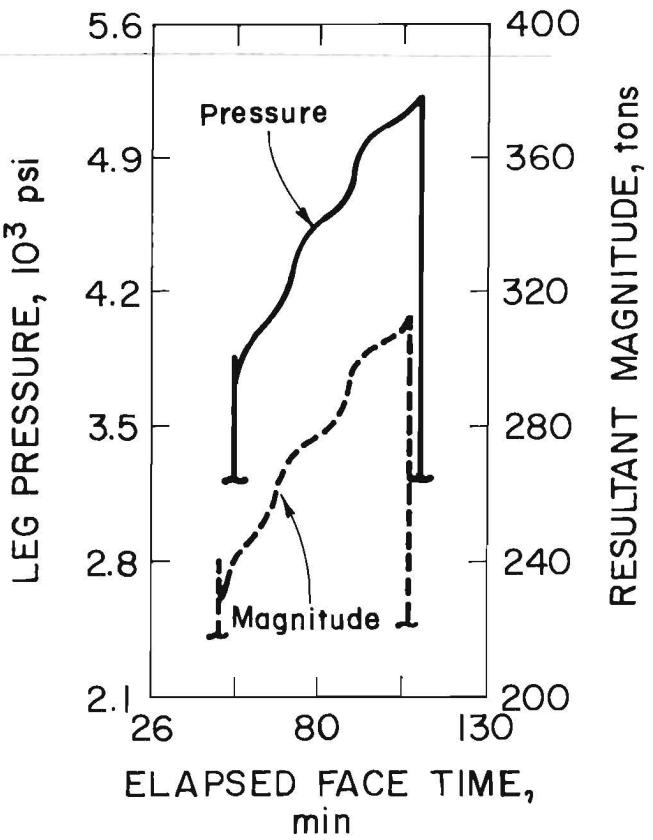

FIGURE 40. - Comparison of leg pressure and resultant magnitude.

where ΔR = change in resultant magnitude,

Rmax = maximum support resistance,

and Rmin = minimum support resistance.

For the shield cycles shown in figure 42, the change in resultant magnitude (ΔR) ranged from 8 to 135 tons. The average change in resultant loading for the 30 shield cycles observed for this particular shield was 113 tons, with a standard deviation of 39 tons.

Since the support loading usually varies continuously with time, support resistance must be weighted by time to produce a meaningful value for average support resistance. This is achieved mathematically by integrating the area under the resultant magnitude curve and then dividing it by the total time to obtain a time-weighted average for support resistance.

$$R_{av} = \int_{t_1}^{t_2} \frac{R(t)\,dt}{T}. \qquad (54)$$

For example, the time-weighted average support resistances for the six shield cycles shown in figure 42 are--

R_1 = 228 tons R_4 = 274 tons

R_2 = 272 tons R_5 = 318 tons

R_3 = 206 tons R_6 = 253 tons

An average of these time-weighted averages produces a good indication of the variation in support loading. For the example just discussed, the average time-weighted average support resistance is 258 tons.

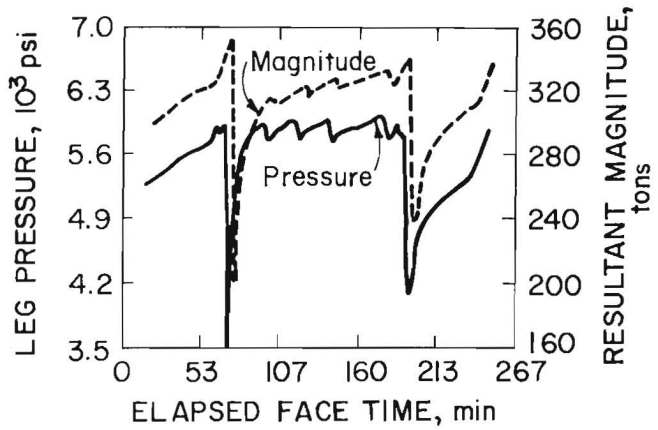

FIGURE 41. - Effect of yielding leg on resultant magnitude.

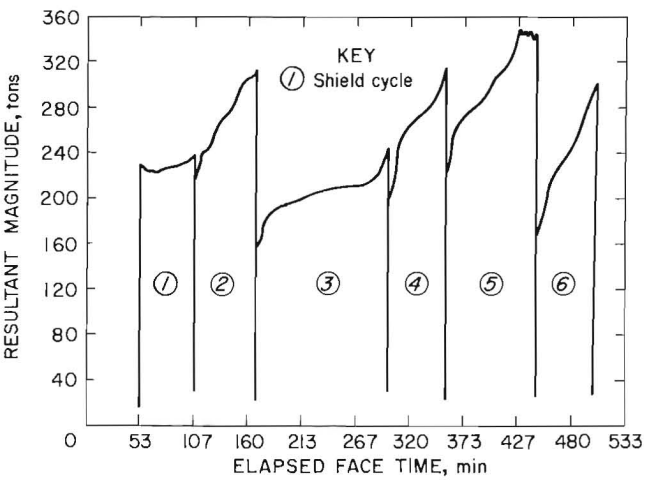

FIGURE 42. - Variation in resultant magnitude shield loading.

Resultant Location

The resultant location exhibited fairly consistent behavior, generally moving toward the rear of the support during the mining cycle. This would be the expected behavior as the strata break and cantilever over the support during the caving process. The position of the resultant load vector stayed relatively close to the leg line, ranging from 3.2 in forward to 2.8 in rearward of the leg line. The leg line is considered the ideal location for the resultant vector, since at this position the leg force would offer maximum support resistance. Positions were found to exist both forward and rearward of the leg line, as well as to cross over the leg line during a particular shield cycle. Statistically, the position of the resultant load vector was determined as follows:

Rear of leg line - 54 pct of shield cycles.

Forward of leg line - 26 pct of shield cycles.

Cross over the leg line - 20 pct of shield cycles.

The variety of resultant load vector locations and their behaviors is illustrated in figure 43, as is the dependence of the resultant location on canopy capsule behavior. Figure 43*A* depicts canopy capsule pressure plotted against time for six shield cycles, while figure 43*B* depicts the resultant location corresponding to the capsule behavior for the same six shield cycles. The position of the leg line is shown by the dash-dot-dash line in figure 43*B* and, as indicated, illustrates cases of resultant location both forward and rearward of the leg line. It is also shown that the position of the resultant vector changes from set to set, owing in part to the dependence of the resultant location on the behavior of the canopy capsule.

By comparing the resultant location with the capsule pressure, it can be seen that as the capsule force (pressure) increases from set to set, the resultant location moves toward the canopy tip; subsequently, as the capsule force decreases, the resultant location moves toward the rear of the support. For example, the large increase in capsule pressure from the second to the third shield cycle (fig. 43) is reflected by a significant movement of the resultant location forward, followed by a movement rearward from the third to fourth shield cycle to reflect decrease in capsule force between these two shield cycles. The influence of the capsule force on the change in resultant location during a shield cycle is also illustrated by examination of the first shield cycle shown in figure 42. Here, it is noticed that a fairly constant capsule pressure resulted in little movement of the resultant location, compared to the consistent rearward movement of the location for the other five shield cycles associated with decreasing capsule pressure. Figure 44 depicts a linear relationship between resultant location and capsule pressure which illustrates that, all other things being held constant (leg force = 353 tons and link force = 118 tons), a change of 0.325 in in the resultant location would

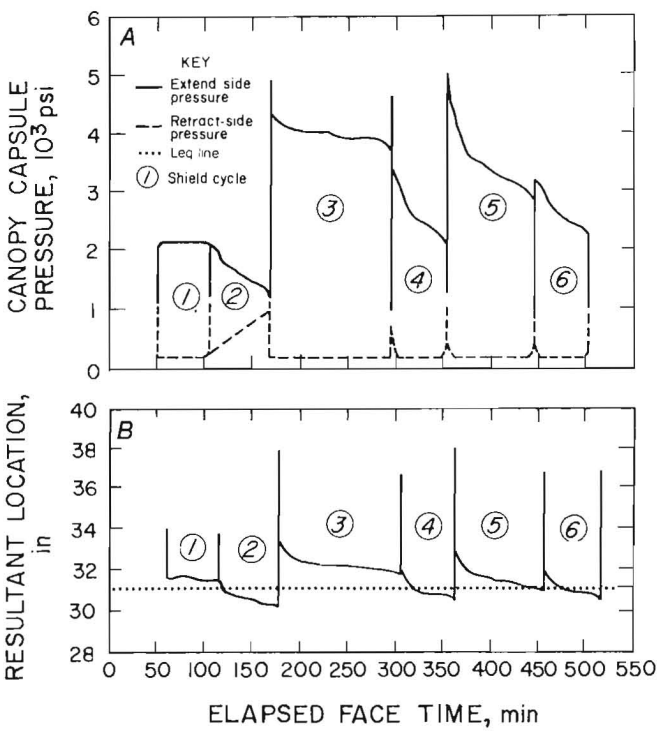

FIGURE 43. - Association between canopy capsule behavior and resultant location.

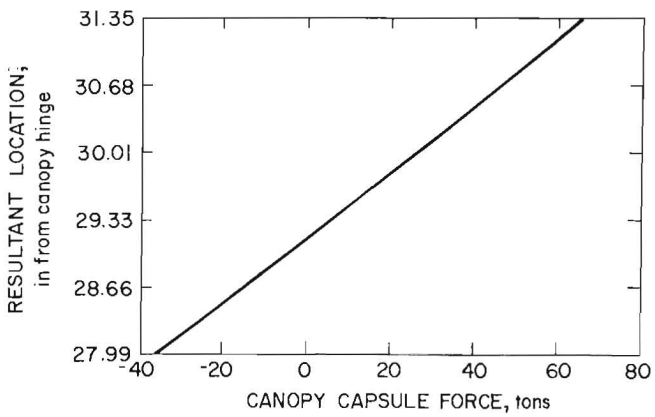

FIGURE 44. - Linear relationship between capsule force and resultant location.

occur for every 10-ton change in canopy capsule pressure. It is also true that leg force has an influence on the behavior of the resultant location, moving the location rearward (i.e., toward the leg line) with an increase in leg force to provide a more efficient support condition. The effect of leg force on resultant location is nonlinear; as shown in figure 45, as the leg force increases, the change in resultant location is less.

Resultant Angle

The resultant angle is a measure of the inclination of the resultant load vector. It is determined by the coefficient of friction produced between the canopy and roof strata caused by horizontal displacement of the strata as well as the reaction of the support to vertical roof convergence. Cases of both high- and low-friction coefficients were observed, but once the support was set, the resultant angle changed very little, indicating the friction coefficient remained constant once the support was "locked in" place, providing a constant of proportionality between horizontal and vertical force. This also indicates there was probably very little horizontal displacement of the strata during the caving process. The resultant angle did change from set to set, ranging from 85° to 107° with 90° representing pure vertical loading. This change from set to set in the direction of the resultant force was probably the result of different contact surfaces providing different frictional forces with each set. These resultant angles produced friction coefficients ranging from 0.07 to 0.36 with typical values ranging from 0.15 to 0.20.

The dominant variable in the resultant angle determination is the lemniscate link force (strain), as illustrated in figure 46, which displays compression lemniscate link strain associated with resultant angle predictions. As indicated in the static analysis of the shield structure, an increase in horizontal load reduced link strain, and as seen in figure 47, as the link strain decreased from the first shield cycle to the second, the resultant angle increased, indicating an increase in horizontal loading. The inverse relationship between link strain and resultant angle is evident in figure 47, where the resultant angle profiles the link strain for the seven shield cycles monitored during that shift. Another observation is that when the resultant angle did change

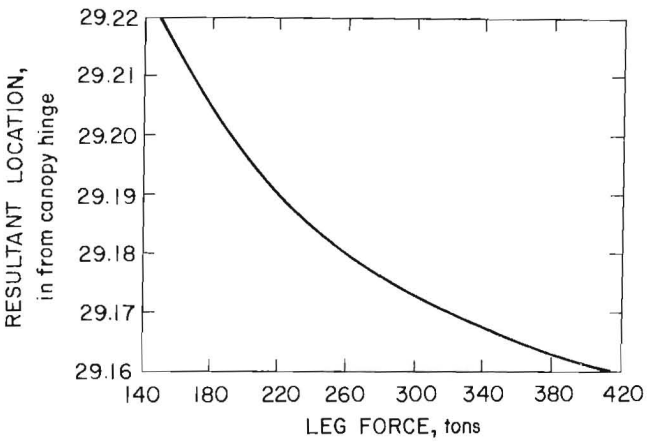

FIGURE 45. - Nonlinear relationship between leg force and resultant location.

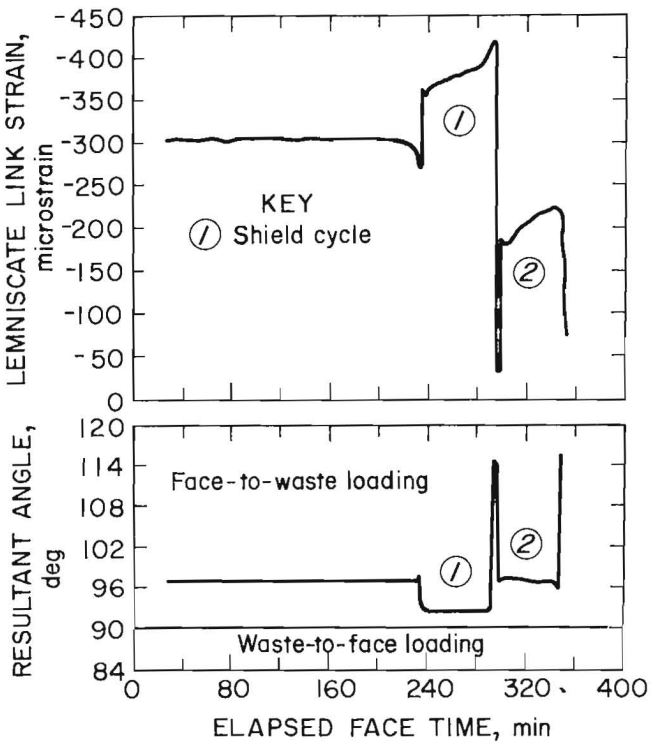

FIGURE 46. - Association between lemniscate link strain and resultant angle.

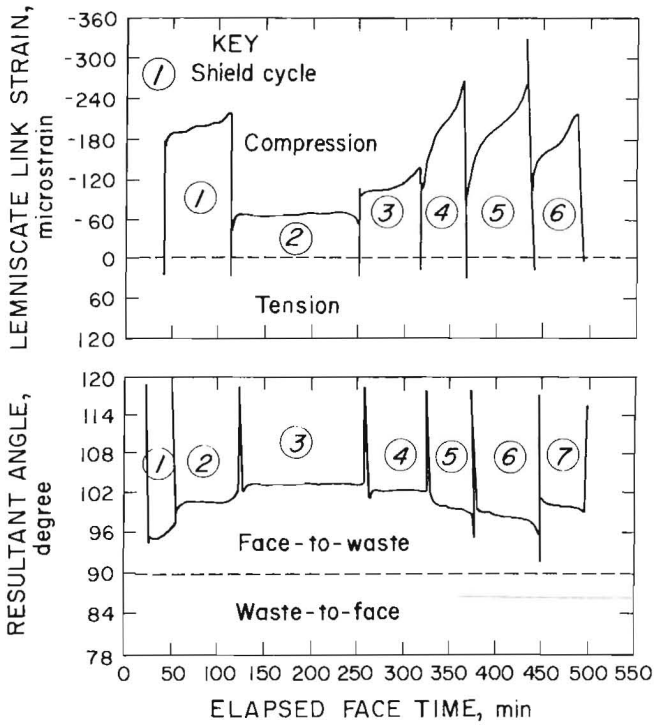

FIGURE 47. - Variation in resultant angle determinations.

during a shield cycle (see cycles 5, 6, and 7 in figure 47), the curve had a shape similar to that for leg pressure, possibly indicating these forces were shield induced as a reaction to vertical roof convergence.

Horizontal Loading

Horizontal load was a primary design consideration for the shield concept, and measurement of actual horizontal load experienced by a longwall shield on an operating face was a primary objective of this project. Horizontal load was found to be present in all shield cycles, ranging in magnitude from 8 to 95 tons. The wide range of magnitudes indicates several loading phenomena were occurring. While there was little consistency in terms of magnitude from shield cycle to shield cycle, horizontal load consistently increased during individual shield cycles. This would be expected, since it is reasonable to assume that the differential displacement of the strata would increase as the caving progressed.

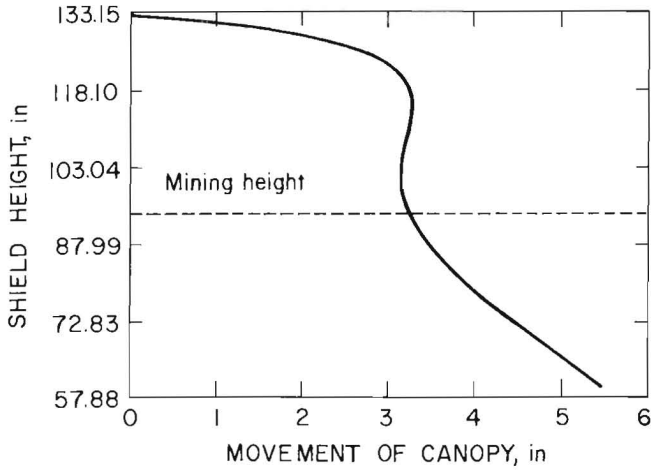

FIGURE 48. - Canopy convergence profile.

However, in terms of measuring horizontal shield loading, one subtle fact must be recognized: Basically, horizontal load is produced any time there is relative motion between the canopy and the base, with sufficient friction to generate a horizontal force between the roof and canopy. This motion can be caused either by horizontal strata displacement trying to push the canopy toward the gob or as a reaction of the support to vertical roof convergence whereby the horizontal component of the leg force tries to induce relative motion between the canopy and base. What we would like to isolate is the roof-generated load due to horizontal strata displacement, since this is the load any support element must resist. In practice, horizontal load is also caused by the shield itself. For example, although the lemniscate system is intended to provide vertical travel of the canopy during convergence, the actual path of the canopy is not truly vertical (fig. 48), and this motion could cause the support to induce a horizontal load into the roof and the shield structure. Likewise, the suppport leg is inclined and also induces a horizontal force into the structure, as a reaction to vertical roof convergence. Hence, it is concluded that horizontal load is both roof generated by horizontal displacement of the strata and shield generated as a reaction of the structure to vertical roof

convergence, and as a result is specific (to some extent) to the design of the particular shield in question.

Like the resultant angle, horizontal force is dependent upon link strain, decreasing in magnitude as the compression lemniscate link strain increases from shield cycle to shield cycle, as shown in figure 49. During the shield cycle, the strain generally increases to reflect the increase in vertical support loading caused by the caving roof, despite the presence of horizontal force that reduces link loading. The variation in horizontal force is shown in figure 50, which depicts horizontal force determinations for the same support for two different shifts. As can be seen from the graphs, there is no time correlation to horizontal loading; rather, the behavior is mostly oriented to geology and roof behavior, owing to the caving mechanism at work.

Since the strains are not very active and have shapes similar to those of leg pressure plots in most instances, there is some evidence that the majority of horizontal force observed at this particular installation was the result of the reaction of the structure to vertical roof convergence and not strata induced by horizontal strata displacements, but the evidence is too inconclusive to make a definitive judgment on the issue.

Vertical Support Resistance

As indicated earlier, the resultant magnitude is comprised of two components: horizontal and vertical loads. It is the vertical component that resists roof convergence and is most often referred to as the measure of support resistance. The shape of the vertical load curve is nearly identical to that of the resultant magnitude curve, as shown in figure 51. The difference between the resultant magnitude and vertical component is relatively small, owing to the sum of the squares of the two components in the resultant relationship $R^2 = Rx^2 + Ry^2$. Unlike horizontal force, which is largely dependent upon link strain, vertical force is almost solely dependent upon leg pressure curves. It was shown earlier in the discussion on shield mechanics that only a relatively small part of the horizontal component of the leg force actually was converted into resistance to horizontal shield loading. However, in the case of vertical force, nearly all the vertical component of the leg force is utilized to resist vertical roof

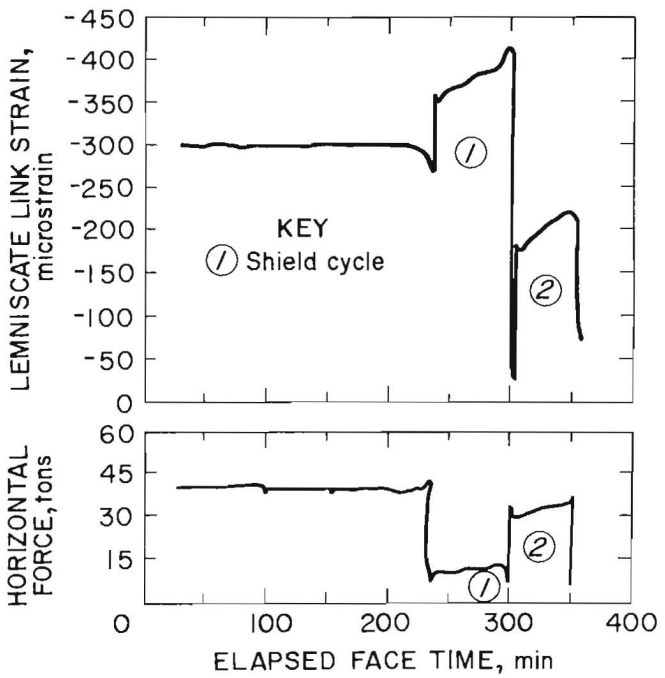

FIGURE 49. - Association between horizontal load and lemniscate link strain.

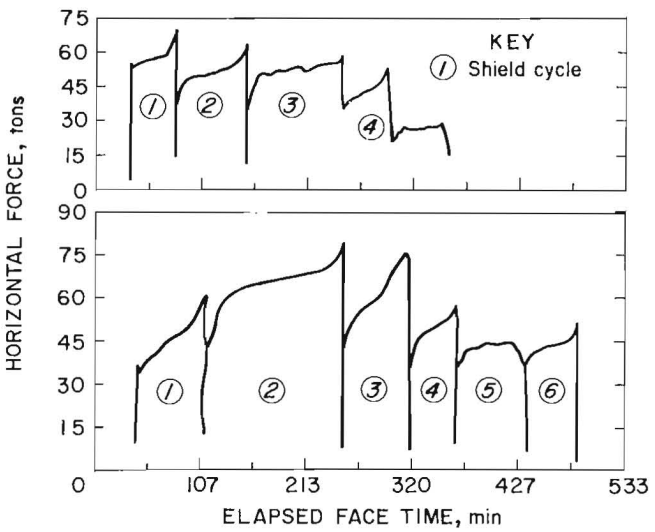

FIGURE 50. - Variation in horizontal force measurements.

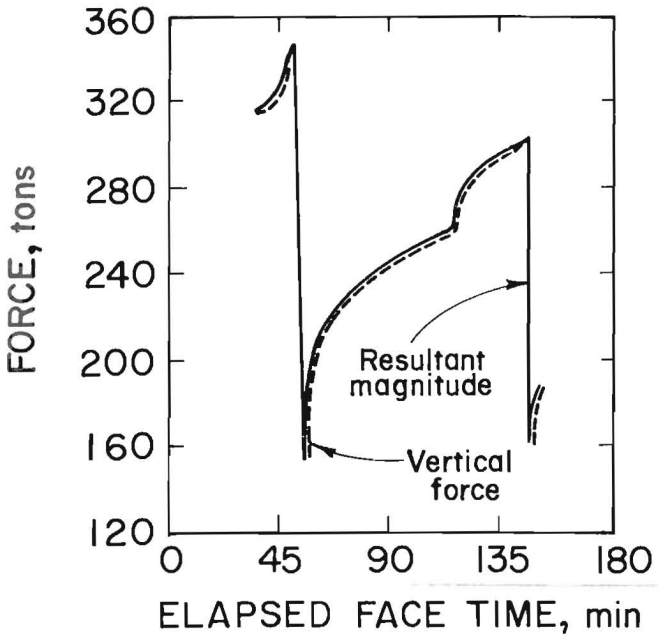

FIGURE 51. - Association between vertical force and resultant magnitude.

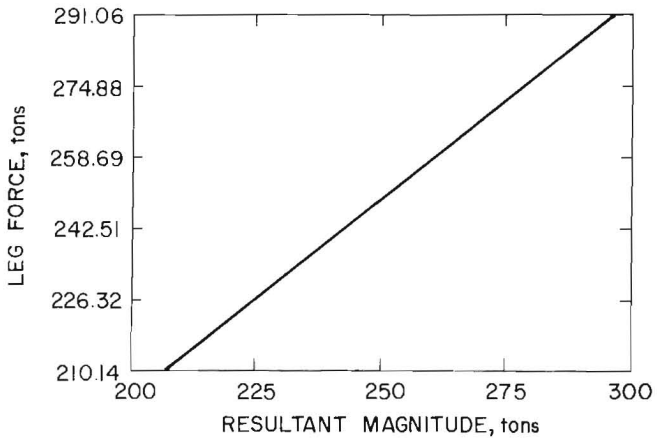

FIGURE 52. - Comparison between vertical leg force and vertical resultant load.

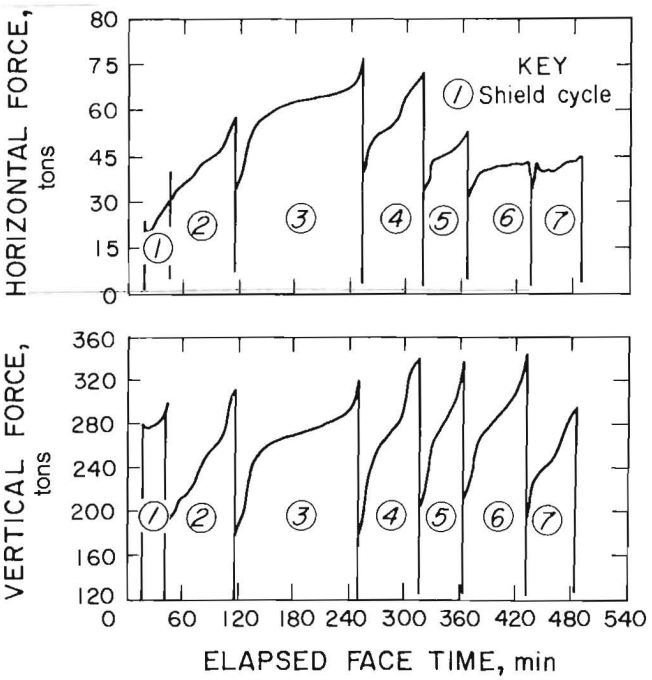

FIGURE 53. - Comparison of vertical and horizontal force.

convergence, producing a slope 0.985 (fig. 52). A perfect correlation would be indicated by a curve of slope 1.0, indicating an equal relationship between the two parameters.

There appears to be a direct shape correspondence between the horizontal predictions and the vertical component of the resultant force. The relationship is clearly not proportional; however, as illustrated in figure 53. The vertical component shapes and magnitudes are similar for shield cycles 4, 5, and 6, but the horizontal component is distinctly different. The larger the link strain, the less proportional the curves become.

If the block being carried by the support were moving only vertically downward, or if its motion followed a linear vertical versus horizontal displacement, then it is likely that horizontal load would be proportional to the vertical load. If the block were detached and free to be displaced horizontally in the face-to-waste direction, there is an increased probability that the proportionality between horizontal and vertical load would no longer be constant. These circumstances would also be indications of strata-induced horizontal loading.

Shield Comparison

As indicated earlier, there were five longwall shields distributed fairly evenly across the face that were instrumented for resultant load studies. The number of samples (shield cycles) taken for each support ranged from 10 to 25 cycles owing to instrumentation problems. Such a small and variable sample size precludes drawing any statistical inferences from

the data, but the general behavior of the individual shields in terms of the resultant load vector parameters can be seen from figure 54. Again, while observations can be made and trends proposed, care must be taken in drawing any generalized conclusions relative to loading conditions distributed about the face. Since the intent of this effort was only to demonstrate the concept and feasibility of determining resultant shield loading, these limitations are justified. Future studies will entail a much broader data base from which conclusions can be drawn regarding the distribution of loading across the face with more confidence.

DISCUSSION OF RESEARCH EFFORTS AND RESULTS

Proper ground control is essential to the success of longwall mining. Improvement in support design or utilization would provide benefits of increased production and reduced capital risk for the longwall operator. While there are several types of roof support designs, the shield concept has gained prominence in the United States in the past decade.

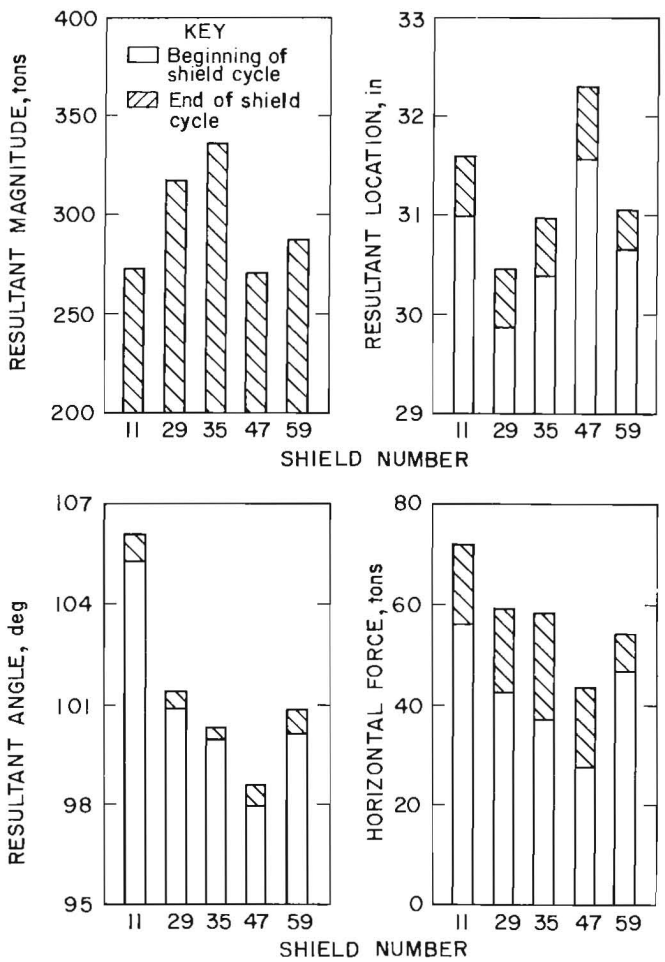

FIGURE 54. - Comparison of resultant load vector parameters among instrumented shields.

The major advantage of the shield design over chocks and frames is its ability to resist horizontal loading. To understand the behavior of the shield concept, it is necessary to understand the mechanics of the shield structure. Kinematically, the shield is an indeterminant structure, and there are several variables that impact the load-carrying capability of the support. Unlike chock supports, support resistance cannot be determined simply from the summation of leg forces.

Static analysis of the shield structure reveals that the resultant load vector can be determined from measurement of the leg, canopy capsule, and compression lemniscate link force. This technique has been successfully tested in the Bureau's Mine Roof Simulator. Results from the laboratory tests indicate that the resultant load vector parameters of magnitude, location, and angle can be reasonably predicted with this method. It has also been demonstrated that the technique can be successfully utilized underground to measure support loading. Resultant load vector measurements from five longwall shields were found to be consistent with shield mechanics and anticipated roof behavior. The technique also proved successful in measuring horizontal shield loading, which is a primary design consideration but a relatively unknown quantity in terms of support behavior. Horizontal load was found to be significant and present on all shield cycles. From the variation in field data, it is apparent that several loading phenomena were occurring during the study. The nature of these data also indicates that both roof- and shield-generated loading profiles were observed. The information gained in terms of the resultant location

and angle provided insight into the interaction of the support with the strata. This information would have been unattainable if only leg pressures had been monitored, as historically has been done in roof support evaluations. Coefficients of friction were successfully determined from the resultant load vector parameters, which heretofore have been largely assumed as 0.3 in analytical analyses of roof support structures. The proximity of the resultant location to the leg line provides valuable design information for support manufacturers, as well as insight into the caving mechanism of the strata. Finally, the load-carrying capability of the support was properly assessed from the resultant magnitude, which considers both vertical and horizontal loading.

The resultant load vector concept and the measurements taken as part of this study are first steps in providing a more in-depth understanding of support behavior and requirements for more effective ground control. Most of the problems experienced in these initial efforts have been instrumentation related, and improved data acquisition hardware will be developed for future studies. The long-range goals of these and similar studies will be to develop criteria for more effective roof support systems and to develop a better predictive model whereby support requirements can be better correlated to geologic conditions and caving mechanisms.

To achieve these goals, it will be necessary to match support requirements with geologic behavior by complementing support loading studies with strata deformation studies. The objectives of the strata deformation studies will be to monitor near-seam strata behavior in terms of displacements, deflections, and strain contours, and to assess the impact of support loading on roof behavior and vice versa. In addition, the resulatnt load vector studies must be expanded to include other mine sites of different geological character to provide a broader data base from which generalized observations can be made and conclusions drawn. In summary, it is thought that these resultant load vector studies will provide advancement in the state of the art of longwall mining and a foundation for additional studies to improve support design.

CONCLUSIONS

The following conclusions are drawn and their significance discussed relative to the efforts of this research to evaluate the mechanics of the shield support and to develop a technique to determine resultant loading:

1. The shield structure is kinematically indeterminant, and resultant shield loading cannot be determined from leg pressure data alone.--The significance of this conclusion is that the historical practice of measuring leg pressure data is inadequate to properly evaluate shield support loading. The resultant load vector has parameters of magnitude, location, and angle of inclination, which require three independent equations for solution.

2. Resultant magnitude can be reasonably estimated from leg pressure data, but estimating resultant location and angle of inclination requires the measurement of canopy capsule and lemniscate link forces.--The implication of this conclusion is that support capacity requirements (ability to resist vertical convergence) can be deduced from leg pressure data. The error in determining resultant magnitude from leg pressure data is likely to be less than the margin of safety coal operators are willing to risk for successful longwall mining. However, from a research viewpoint, with a goal of improving support design, the behavior of a shield support cannot be properly assessed unless the resultant forces (magnitude, location, and direction) are accurately known. Critical performance parameters (such as support stability) are dependent upon the location and direction of forces acting on the support as well as their magnitudes. Also, structurally the support capabilities cannot be properly evaluated from vertical loading alone.

3. The load-carrying capability of a shield support is influenced by the presence of horizontal loading.--Horizontal load can either increase or decrease shield capacity, depending upon the location of the instantaneous center of the lemniscate links relative to the plane of the canopy and the particular support configuration. Since manufacturers generally quote support capacity in terms of vertical support loading only, the influence of horizontal loading should be considered in support selection. The operating height at which the support is employed can also be critical to successful operation because of this phenomenon.

4. With a planar static model (two-dimensional), resultant loading on shield supports can be determined by measurement of leg, canopy capsule, and lemniscate link forces.--The significance of this conclusion is twofold: (1) Resultant loading is fundamental to support design, and (2) resultant loading can be determined from a relatively small array of transducers. An effective support design can only be achieved if the resultant forces acting on the support are known. Theoretical studies that evaluate support design are only as good as the accuracy of the load cases simulated. The ability to determine resultant shield loading with a small array of transducers (eight in a two-leg design) limits data acquisition requirements and makes this technique attractive for underground research.

5. The feasibility of employing this technique to measure support loading underground on active longwall shields has been demonstrated.--Five longwall shields were instrumented with pressure transducers and strain gauges, and successful resultant load vector determinations were made, providing confidence for future research efforts.

6. Resultant loading field measurements were consistent with theoretical studies of support behavior.--Associations between resultant magnitudes and leg pressure, resultant location and canopy capsule force, and resultant direction and lemniscate link force were observed from the field data, thereby providing evidence that the theoretical hypothesis upon which this research is founded is valid.

7. Initial field measurements produced physically realistic resultant support loading consistent with anticipated mine roof behavior.

A. Resultant magnitudes increased as a function of time, reaching yield capacity of the support on several occasions.

B. Resultant location was near the leg line and moved toward the rear of the support as the strata caved.

C. Resultant inclination remained fairly constant during a shield cycle, indicating that the friction coefficient changed very little once the support was "locked" in place. Coefficients of friction ranged from 0.07 to 0.36 with 0.20 being representative of observed shield loading and strata contact.

8. Horizontal load was found to be present in all shield cycles, ranging in magnitude from 8 to 95 tons.--The basis for design of the shield support is its ability to resist horizontal loading. Despite this being a critical design parameter, horizontal loading produced by the caving strata has been a relatively unknown quantity. The significance of these results is that horizontal load does exist and is of sufficient magnitude to warrant design consideration.

9. There is some evidence that indicates that the majority of observed horizontal load is shield induced by a reaction to vertical roof convergence rather than roof induced due to horizontal strata displacement.--If it can be proved that horizontal strata activity is minimal and that the majority of horizontal loading is support-induced as a reaction to vertical roof convergence, the impact on support design can be far reaching. The presence of horizontal load was a significant discovery, but the more important issue is the source of this loading. If horizontal loading is primarily due to vertical roof convergence, then the shield support is an inefficient design and the concept of the shield design might need to be reevaluated. Although there is some evidence to indicate the majority of the load observed during this study was shield generated, this evidence

is not conclusive and does not mean that this would be a universal behavior representative of all longwall mining conditions. More studies need to be made to determine the source and nature of horizontal shield loading, since the potential exists to dramatically improve support design through these studies.

10. The potential exists to utilize supports as monitors to assess roof and strata behavior.--Knowledge of the resultant location and angle of inclination can provide insight into the behavior of the roof during the caving process. Periodic weighting by measurement of resultant support loading can also provide information on the caving mechanism. Analytical studies involving support evaluations typically utilize the weight of a trapezoidal rock mass for support loading, ignoring the movement of that mass, which would provide a horizontal component to the resulting force. Correlations could also be made from the resultant load determinations regarding the height and overhang of the caving strata from the resultant support loading. Knowledge of horizontal loading will provide indications of near-seam strata activity in terms of face-to-waste displacement of the strata along bedding planes.

FUTURE EFFORTS

Much has been learned from these initial research efforts to develop techniques to properly assess shield loading, but several new questions have been revealed and additional work needs to be done to realize the benefits of this research. Future research efforts are outlined as follows:

1. Studies will be undertaken in the MRS to evaluate the potential sources of horizontal support loading. Underground experiments will be planned to specifically evaluate strata movements and support behavior to ascertain the degree of strata-induced horizontal shield loading.

2. Resultant load vector measurements need to be made at other mine sites of differing geologic character to provide a larger data base for analysis of support behavior.

3. Permissible digital data acquisition instrumentation will be developed to facilitate monitoring several shields for expanded underground studies.

4. Support loading efforts need to be expanded to include monitoring several shields over the life of the panel to evaluate such factors as first break and the effect of periodic weighting on support behavior.

5. Support loading studies will be complemented with strata deformation studies to provide additional insight into the interaction of the support with strata activity.

REFERENCES

1. Barczak, T. M., and R. C. Garson. Technique to Measure Resultant Load Vector on Shield Supports. Pres. at 25th U.S. Symp. on Rock Mechanics in Productivity and Protection, Evanston, IL, June 25-27, 1984, pp. 667-680; available upon request from T. M. Barczak, BuMines, Pittsburgh, PA.

2. Barczak, T. M., R. C. Garson, P. M. Yavorsky, and F. S. Maayeh. State-of-the-Art Testing of Powered Roof Supports. Pres. at 2d Conf. on Ground Control in Mining, Morgantown, WV, July 19-21, 1982, pp. 64-77; available upon request from T. M. Barczak, BuMines, Pittsburgh, PA.

3. Peng, S. S. Coal Mine Ground Control. Wiley, 1978, pp. 232-268.

4. Jackson, D. H. The Testing of Shield Supports. Min. Eng. (Littleton, CO), v. 138, Apr. 1979, pp. 1-7.

5. Peng, S. S. Longwall Mining. Wiley, 1984, pp. 239-244.

APPENDIX.--NOMENCLATURE

A - Cross-sectional area.

α - Leg angle normal to plane of canopy.

ANG - Resultant angle.

C - Compression lemniscate link force.

E - Modulus of elasticity.

ε - Microstrain.

FM - Frequency modulated.

G_x - Horizontal component of resultant gob load acting on caving shield.

G_y - Vertical component of resultant gob load acting on caving shield.

HORZ - Horizontal shield load.

H_1 - Horizontal load acting on canopy.

H_2 - Horizontal load acting on base.

I_x - Moment of inertia.

L - Leg force.

LOC - Resultant location.

LOC 1 - Resultant location on canopy.

LOC 2 - Resultant location on base.

L_x - Horizontal component of leg force.

L_y - Vertical component of leg force.

MAG - Resultant magnitude.

N - Canopy capsule force.

N_x - Horizontal component of canopy capsule force.

N_y - Vertical component of canopy capsule force.

P_x - Horizontal component of canopy hinge pin reaction load.

P_y - Vertical component of canopy hinge pin reaction load.

R - Resultant load.

σ - Stress.

θ - Canopy capsule angle normal to plane of canopy.

T - Tension lemniscate link force.

VERT - Vertical shield load.

VF - Arbitrary vector parameter equation.

V_1 - Vertical resultant load acting on canopy.

V_2 - Vertical resultant load acting on base.

X_g, Y_g - Spatial coordinates defining location of resultant gob load.

INT.-BU.OF MINES,PGH.,PA. 28282

☆ U.S. GOVERNMENT PRINTING OFFICE: 1986—605-017/40,043